
Variational f -Divergence and Derangements for Discriminative Mutual Information Estimation

Nunzio A. Letizia, Nicola Novello, Andrea M. Tonello

Institute of Networked and Embedded Systems

University of Klagenfurt, Austria

{nunzio.letizia},{nicola.novello},{andrea.tonello}@aau.at

Abstract

The accurate estimation of the mutual information is a crucial task in various applications, including machine learning, communications, and biology, since it enables the understanding of complex systems. High-dimensional data render the task extremely challenging due to the amount of data to be processed and the presence of convoluted patterns. Neural estimators based on variational lower bounds of the mutual information have gained attention in recent years but they are prone to either high bias or high variance as a consequence of the partition function. We propose a novel class of discriminative mutual information estimators based on the variational representation of the f -divergence. We investigate the impact of the permutation function used to obtain the marginal training samples and present a novel architectural solution based on derangements. The proposed estimator is flexible as it exhibits an excellent bias/variance trade-off. Experiments on reference scenarios demonstrate that our approach outperforms state-of-the-art neural estimators both in terms of accuracy and complexity.

1 Introduction

The mutual information (MI) between two multivariate random variables, X and Y , is a fundamental quantity in statistics, representation learning, information theory, communication engineering and biology [1, 2, 3, 4]. It quantifies the statistical dependence between X and Y by measuring the amount of information obtained about X via the observation of Y , and it is defined as

$$I(X; Y) = \mathbb{E}_{(\mathbf{x}, \mathbf{y}) \sim p_{XY}(\mathbf{x}, \mathbf{y})} \left[\log \frac{p_{XY}(\mathbf{x}, \mathbf{y})}{p_X(\mathbf{x})p_Y(\mathbf{y})} \right]. \quad (1)$$

Unfortunately, computing $I(X; Y)$ is challenging since the joint probability density function $p_{XY}(\mathbf{x}, \mathbf{y})$ and the marginals $p_X(\mathbf{x})$, $p_Y(\mathbf{y})$ are usually unknown, especially when dealing with high-dimensional data. Some recent techniques [5, 6] have demonstrated that neural networks can be leveraged as probability density function estimators and, more in general, are capable of modeling the data dependence. Discriminative approaches [7, 8] compare samples from both the joint and marginal distributions to directly compute the density ratio (or the log-density ratio)

$$R(\mathbf{x}, \mathbf{y}) = \frac{p_{XY}(\mathbf{x}, \mathbf{y})}{p_X(\mathbf{x})p_Y(\mathbf{y})}. \quad (2)$$

Generative approaches [9, 10], instead, aim at modeling the individual densities. We focus on discriminative MI estimation since it can in principle enjoy some of the properties of implicit generative models, which are able of directly generating data that belongs to the same distribution of the input data without any explicit density estimate. In this direction, the most successful technique is represented by generative adversarial networks (GANs) [11]. The adversarial training pushes the

discriminator $D(\mathbf{x})$ towards the optimum value

$$\hat{D}(\mathbf{x}) = \frac{p_{data}(\mathbf{x})}{p_{data}(\mathbf{x}) + p_{gen}(\mathbf{x})} = \frac{1}{1 + \frac{p_{gen}(\mathbf{x})}{p_{data}(\mathbf{x})}}. \quad (3)$$

Therefore, the output of the optimum discriminator is itself a function of the density ratio p_{gen}/p_{data} , where p_{gen} and p_{data} are the distributions of the generated and the collected data, respectively.

We generalize the observation of (3) and we propose a family of MI estimators based on the variational lower bound of the f -divergence [12, 13]. In particular, we argue that the maximization of any f -divergence variational lower bound can lead to a MI estimator with excellent bias/variance trade-off.

Since we typically have access only to joint data points $(\mathbf{x}, \mathbf{y}) \sim p_{XY}(\mathbf{x}, \mathbf{y})$, another relevant practical aspect is the sampling strategy to obtain data from the product of marginals $p_X(\mathbf{x})p_Y(\mathbf{y})$, for instance via a shuffling mechanism along N realizations of Y . We analyze the impact that the permutation has on the training and we propose a derangement training strategy that achieves high performance requiring $\Omega(N)$ operations. Simulation results demonstrate that the proposed approach exhibits improved estimations in a multitude of scenarios.

In brief, we can summarize our contributions over the state-of-the-art as follows:

- For any f -divergence, we derive a training value function whose maximization leads to a given MI estimator.
- We compare different f -divergences and comment on the resulting estimator properties and performance.
- We propose a novel derangement training strategy that provides unbounded MI estimation, differently from a random permutation function.
- We unify the main discriminative estimators into a publicly available code which can be used to reproduce all the results of this paper.

2 Related Work

Traditional approaches for the MI estimation rely on binning, density and kernel estimation [14] and k -nearest neighbors [15]. Nevertheless, they do not scale to problems involving high-dimensional data as it is the case in modern machine learning applications. Hence, deep neural networks have recently been leveraged to maximize variational lower bounds on the MI [12, 16, 17]. The expressive power of neural networks has shown promising results in this direction although less is known about the effectiveness of such estimators [18], especially since they suffer from either high bias or high variance.

The discriminative approach usually exploits an energy-based variational family of functions to provide a lower bound on the Kullback-Leibler (KL) divergence. As an example, the Donsker-Varadhan dual representation of the KL divergence [12, 19] produces an estimate of the MI using the bound optimized by the mutual neural information estimator (MINE) [17]

$$I_{MINE}(X; Y) = \sup_{\theta \in \Theta} \mathbb{E}_{(\mathbf{x}, \mathbf{y}) \sim p_{XY}(\mathbf{x}, \mathbf{y})} [T_{\theta}(\mathbf{x}, \mathbf{y})] - \log(\mathbb{E}_{(\mathbf{x}, \mathbf{y}) \sim p_X(\mathbf{x})p_Y(\mathbf{y})} [e^{T_{\theta}(\mathbf{x}, \mathbf{y})}]), \quad (4)$$

where $\theta \in \Theta$ parameterizes a family of functions $T_{\theta} : \mathcal{X} \times \mathcal{Y} \rightarrow \mathbb{R}$ through the use of a deep neural network. However, Monte Carlo sampling renders MINE a biased estimator. To avoid biased gradients, the authors in [17] suggested to replace the partition function $\mathbb{E}_{p_X p_Y} [e^{T_{\theta}}]$ with an exponential moving average over mini-data-batches.

Another variational lower bound is based on the KL divergence dual representation introduced in [16] (also referred to as f -MINE in [17])

$$I_{NWJ}(X; Y) = \sup_{\theta \in \Theta} \mathbb{E}_{(\mathbf{x}, \mathbf{y}) \sim p_{XY}(\mathbf{x}, \mathbf{y})} [T_{\theta}(\mathbf{x}, \mathbf{y})] - \mathbb{E}_{(\mathbf{x}, \mathbf{y}) \sim p_X(\mathbf{x})p_Y(\mathbf{y})} [e^{T_{\theta}(\mathbf{x}, \mathbf{y}) - 1}]. \quad (5)$$

Although MINE provides a tighter bound $I_{MINE} \geq I_{NWJ}$, the NWJ estimator is unbiased.

Both MINE and NWJ suffer from high-variance estimations and to combat such a limitation, the SMILE estimator was introduced in [18]. It is defined as

$$I_{SMILE}(X; Y) = \sup_{\theta \in \Theta} \mathbb{E}_{(\mathbf{x}, \mathbf{y}) \sim p_{XY}(\mathbf{x}, \mathbf{y})} [T_{\theta}(\mathbf{x}, \mathbf{y})] - \log(\mathbb{E}_{(\mathbf{x}, \mathbf{y}) \sim p_X(\mathbf{x})p_Y(\mathbf{y})} [\text{clip}(e^{T_{\theta}(\mathbf{x}, \mathbf{y})}, e^{-\tau}, e^{\tau})]), \quad (6)$$

where $\text{clip}(v, l, u) = \max(\min(v, u), l)$ and it helps to obtain smoother partition functions estimates. SMILE is equivalent to MINE in the limit $\tau \rightarrow +\infty$.

The MI estimator based on contrastive predictive coding (CPC) [20] is defined as

$$I_{CPC}(X; Y) = \mathbb{E}_{(\mathbf{x}, \mathbf{y}) \sim p_{XY, N}(\mathbf{x}, \mathbf{y})} \left[\frac{1}{N} \sum_{i=1}^N \log \left(\frac{e^{T_{\theta}(\mathbf{x}_i, \mathbf{y}_i)}}{\frac{1}{N} \sum_{j=1}^N e^{T_{\theta}(\mathbf{x}_i, \mathbf{y}_j)}} \right) \right], \quad (7)$$

where N is the batch size and $p_{XY, N}$ denotes the joint distribution of N i.i.d. random variables sampled from p_{XY} . CPC provides low variance estimates but it is upper bounded by $\log N$, resulting in a biased estimator.

Another estimator based on a classification task is the neural joint entropy estimator (NJEE) proposed in [21]. Let X_m be the m -th component of X , with $m \leq d$ and N the batch size. X^k is the vector containing the first k components of X . Let $\hat{H}_N(X_1)$ be the estimated marginal entropy of the first components in X and let $G_{\theta_m}(X_m | X^{m-1})$ be a neural network classifier, where the input is X^{m-1} and the label used is X_m . If $\text{CE}(\cdot)$ is the cross-entropy function, then the MI estimator based on NJEE is defined as

$$I_{NJEE}(X; Y) = \hat{H}_N(X_1) + \sum_{m=2}^d \text{CE}(G_{\theta_m}(X_m | X^{m-1})) - \sum_{m=1}^d \text{CE}(G_{\theta_m}(X_m | Y, X^{m-1})), \quad (8)$$

where the first two terms of the RHS constitutes the NJEE estimator.

Inspired by the f -GAN training objective [22], in the following, we present a class of discriminative MI estimators based on the f -divergence measure. Conversely to what has been proposed so far in the literature, where f is always constrained to be the generator of the KL divergence, we allow for any choice of f . Different f functions will have different impact on the training and optimization sides, while on the estimation side, the partition function does not need to be computed, leading to low variance estimators.

Notation and Remarks

X denotes a multivariate random variable (random vector) of dimension d , while $\mathbf{x} \in \mathcal{X}$ denotes its realization. $p_Y(\mathbf{y}|\mathbf{x})$ and $p_{XY}(\mathbf{x}, \mathbf{y})$ represent the conditional and joint probability density or mass functions, while $p_X(\mathbf{x})p_Y(\mathbf{y})$ is the product of the two marginals probability functions. $\log(\cdot)$ denotes the natural logarithm while $I(X; Y)$ denotes the mutual information between the random variables X and Y . Lastly, $D_{\text{KL}}(p||q)$ is the Kullback-Leibler (KL) divergence of the distribution p from q .

All lemmas and theorems are proved in the Appendix.

3 f -Divergence Mutual Information Estimation

The calculation of the MI via a discriminative approach requires the density ratio (2). From (3), we observe that $I(X; Y)$ can be estimated using the optimum discriminator \hat{D} when $p_{data} \equiv p_X p_Y$ and $p_{gen} \equiv p_{XY}$. Notice that the optimal output is not directly in the form needed for the MI estimation, namely, $p_{XY}/(p_X p_Y)$, rather it is a non-linear invertible function of the density ratio, in fact, $p_{XY}/(p_X p_Y) = (1 - D)/D$. In the following, we show that any variational representation of the f -divergence serves our purpose. Consequently, the optimum discriminator can be formulated in various forms based on the selected f -divergence, leading to a whole set of new estimators.

The authors in [22] extended the variational divergence estimation framework presented in [16] and showed that any f -divergence can be used to train GANs. Inspired by such idea, we now argue that also discriminative MI estimators enjoy similar properties if the variational representation of f -divergence functionals $D_f(P||Q)$ is adopted.

In detail, let P and Q be absolutely continuous measures w.r.t. dx and assume they possess densities p and q , then the f -divergence is defined as follows

$$D_f(P||Q) = \int_{\mathcal{X}} q(\mathbf{x}) f\left(\frac{p(\mathbf{x})}{q(\mathbf{x})}\right) d\mathbf{x}, \quad (9)$$

where \mathcal{X} is a compact domain and the function $f : \mathbb{R}_+ \rightarrow \mathbb{R}$ is convex, lower semicontinuous and satisfies $f(1) = 0$.

The following theorem introduces f -DIME, a class of discriminative mutual information estimators (DIME) based on the variational representation of the f -divergence.

Theorem 1. *Let $(X, Y) \sim p_{XY}(\mathbf{x}, \mathbf{y})$ be a pair of multivariate random variables. Let $\sigma(\cdot)$ be a permutation function such that $p_{\sigma(Y)}(\sigma(\mathbf{y})|\mathbf{x}) = p_Y(\mathbf{y})$. Let f^* be the Fenchel conjugate of $f : \mathbb{R}_+ \rightarrow \mathbb{R}$, a convex lower semicontinuous function that satisfies $f(1) = 0$ with derivative f' . If $\mathcal{J}_f(T)$ is a value function defined as*

$$\mathcal{J}_f(T) = \mathbb{E}_{(\mathbf{x}, \mathbf{y}) \sim p_{XY}(\mathbf{x}, \mathbf{y})} \left[T(\mathbf{x}, \mathbf{y}) - f^* \left(T(\mathbf{x}, \sigma(\mathbf{y})) \right) \right], \quad (10)$$

then

$$\hat{T}(\mathbf{x}, \mathbf{y}) = \arg \max_T \mathcal{J}_f(T) = f' \left(\frac{p_{XY}(\mathbf{x}, \mathbf{y})}{p_X(\mathbf{x})p_Y(\mathbf{y})} \right), \quad (11)$$

and

$$I(X; Y) = I_{fDIME}(X; Y) = \mathbb{E}_{(\mathbf{x}, \mathbf{y}) \sim p_{XY}(\mathbf{x}, \mathbf{y})} \left[\log \left((f^*)'(\hat{T}(\mathbf{x}, \mathbf{y})) \right) \right]. \quad (12)$$

We propose to parametrize $T(\mathbf{x}, \mathbf{y})$ with a deep neural network T_θ of parameters θ and solve with gradient ascent and back-propagation to obtain

$$\hat{\theta} = \arg \max_{\theta} \mathcal{J}_f(T_\theta). \quad (13)$$

By doing so, it is possible to guarantee (see Lemma 3 in Sec. B of the Appendix) that, at every training iteration n , the convergence of the f -DIME estimator $\hat{I}_{n, fDIME}(X; Y)$ is controlled by the convergence of T towards the tight bound \hat{T} while maximizing $\mathcal{J}_f(T)$.

Theorem 1 shows that any value function \mathcal{J}_f of the form in (10), seen as the dual representation of a given f -divergence D_f , can be maximized to estimate the MI via (12). It is interesting to notice that the proposed class of estimators does not need any evaluation of the partition term.

It is also important to remark the difference between the classical variational lower bounds estimators that follow a discriminative approach and the DIME-like estimators. They both achieve the goal through a discriminator network that outputs a function of the density ratio. However, the former models exploit the variational representation of the MI (or the KL) and, at the equilibrium, use the discriminator output directly in one of the value functions presented in Sec. 2. The latter, instead, use the variational representation of *any* f -divergence to extract the density ratio estimate directly from the discriminator output.

In the upcoming sections, we analyze the variance of f -DIME and we propose a training strategy for the implementation of Theorem 1. In our experiments, we consider the cases when f is the generator of: a) the KL divergence; b) the GAN divergence; c) the Hellinger distance squared. Due to space constraints, we report in Sec. A of the Appendix the value functions used for training and the mathematical expressions of the resulting DIME estimators.

4 Variance Analysis

In this section, we assume that the ground truth density ratio $\hat{R}(\mathbf{x}, \mathbf{y})$ exists and corresponds to the density ratio in (2). We also assume that the optimum discriminator $\hat{T}(\mathbf{x}, \mathbf{y})$ is known and already obtained (e.g. via a neural network parametrization).

We define $p_{XY}^M(\mathbf{x}, \mathbf{y})$ and $p_X^N(\mathbf{x})p_Y^N(\mathbf{y})$ as the empirical distributions corresponding to M i.i.d. samples from the true joint distribution p_{XY} and to N i.i.d. samples from the product of marginals $p_X p_Y$, respectively. The randomness of the sampling procedure and the batch sizes M, N influence the variance of variational MI estimators. In the following, we prove that under the previous assumptions, f -DIME exhibits better performance in terms of variance w.r.t. some variational estimators with a discriminative approach, e.g., MINE and NWJ.

The partition function estimation $\mathbb{E}_{p_X^N p_Y^N}[\hat{R}]$ represents the major issue when dealing with variational MI estimators. Indeed, they comprise the evaluation of two terms (using the given density ratio), and the partition function is the one responsible for the variance growth. The authors in [18] characterized the variance of both MINE and NWJ estimators, in particular, they proved that the variance scales exponentially with the ground-truth MI $\forall M \in \mathbb{N}$

$$\begin{aligned} \text{Var}_{p_{XY}, p_{XPY}} [I_{NWJ}^{M,N}] &\geq \frac{e^{I(X;Y)} - 1}{N} \\ \lim_{N \rightarrow \infty} N \text{Var}_{p_{XY}, p_{XPY}} [I_{MINE}^{M,N}] &\geq e^{I(X;Y)} - 1, \end{aligned} \quad (14)$$

where

$$\begin{aligned} I_{NWJ}^{M,N} &:= \mathbb{E}_{p_{XY}^M} [\log \hat{R} + 1] - \mathbb{E}_{p_X^N p_Y^N} [\hat{R}] \\ I_{MINE}^{M,N} &:= \mathbb{E}_{p_{XY}^M} [\log \hat{R}] - \log \mathbb{E}_{p_X^N p_Y^N} [\hat{R}]. \end{aligned} \quad (15)$$

To reduce the impact of the partition function on the variance, the authors of [18] also proposed to clip the density ratio between $e^{-\tau}$ and e^τ leading to an estimator (SMILE) with bounded partition variance. However, also the variance of the log-density ratio $\mathbb{E}_{p_{XY}^M} [\log \hat{R}]$ influences the variance of the variational estimators, since it is clear that

$$\text{Var}_{p_{XY}, p_{XPY}} [I_{VLB}^{M,N}] \geq \text{Var}_{p_{XY}} [\mathbb{E}_{p_{XY}^M} [\log \hat{R}]], \quad (16)$$

a result that holds in general for any type of variational MI lower bound (VLB) based estimator.

The great advantage of f -DIME is to avoid the partition function estimation step, significantly reducing the variance of the estimator. Under the same initial assumptions, from (16) we can immediately conclude that

$$\text{Var}_{p_{XY}} [I_{fDIME}^M] \leq \text{Var}_{p_{XY}, p_{XPY}} [I_{VLB}^{M,N}], \quad (17)$$

where

$$I_{fDIME}^M := \mathbb{E}_{p_{XY}^M} [\log \hat{R}] \quad (18)$$

is the Monte Carlo implementation of f -DIME. Hence, the f -DIME class of models has lower variance than any VLB based estimator (MINE, NWJ, SMILE, etc.). The following lemma provides an upper bound on the variance of the f -DIME estimator. Notice that such result holds for any type of value function \mathcal{J}_f , so it is not restrictive to the KL divergence.

Lemma 1. *Let $\hat{R} = p_{XY}(\mathbf{x}, \mathbf{y}) / (p_X(\mathbf{x})p_Y(\mathbf{y}))$ be the density ratio and assume $\text{Var}_{p_{XY}} [\log \hat{R}]$ exists. Let p_{XY}^M be the empirical distribution of M i.i.d. samples from p_{XY} and let $\mathbb{E}_{p_{XY}^M}$ denote the sample average over p_{XY}^M . Then, under the randomness of the sampling procedure it follows that*

$$\text{Var}_{p_{XY}} [\mathbb{E}_{p_{XY}^M} [\log \hat{R}]] \leq \frac{4H^2(p_{XY}, p_{XPY}) \left\| \frac{p_{XY}}{p_X p_Y} \right\|_\infty - I^2(X; Y)}{M} \quad (19)$$

where H^2 is the Hellinger distance squared.

We provide in the Appendix (see Lemma 4) a characterization of the variance of the estimator in (18) when X and Y are correlated Gaussian random variables. We found out that the variance is finite and we use this theoretical result to verify in the experiments that the variance of f -DIME does not diverge for high values of MI.

5 Derangement Strategy

The discriminative approach essentially compares expectations over both joint $(\mathbf{x}, \mathbf{y}) \sim p_{XY}$ and marginal $(\mathbf{x}, \mathbf{y}) \sim p_X p_Y$ data points. However, the samples are derived from the joint distribution and therefore a shuffling mechanism for the realizations of either X or Y is typically deployed to break the joint relationship and get marginal samples. We study the structure that the permutation law $\sigma(\cdot)$ in Theorem 1 needs to have when numerically implemented. In particular, we now prove

that a naive permutation over the realizations of Y results in an incorrect variational lower bound of the f -divergence, causing the MI estimator to be bounded by $\log(N)$, where N is the batch size. To solve this issue, we propose a derangement strategy.

Let the data points $(\mathbf{x}, \mathbf{y}) \sim p_{XY}$ be N pairs $(\mathbf{x}_i, \mathbf{y}_i), \forall i \in \{1, \dots, N\}$. The naive permutation of \mathbf{y} , denoted as $\pi(\mathbf{y})$, leads to N new random pairs $(\mathbf{x}_i, \mathbf{y}_j), \forall i$ and $j \in \{1, \dots, N\}$. The idea is that a random naive permutation may lead to at least one pair $(\mathbf{x}_k, \mathbf{y}_k)$, with $k \in \{1, \dots, N\}$, which is actually a sample from the joint distribution. Viceversa, the derangement of \mathbf{y} , denoted as $\delta(\mathbf{y})$, leads to N new random pairs $(\mathbf{x}_i, \mathbf{y}_j)$ such that $i \neq j, \forall i$ and $j \in \{1, \dots, N\}$. Such pairs $(\mathbf{x}_i, \mathbf{y}_j), i \neq j$ can effectively be considered samples from $p_X(\mathbf{x})p_Y(\mathbf{y})$.

The following lemma analyzes the relationship between the Monte Carlo approximations of the variational lower bounds of the f -divergence \mathcal{J}_f in Theorem 1 using $\pi(\cdot)$ and $\delta(\cdot)$ as permutation laws.

Lemma 2. *Let $(\mathbf{x}_i, \mathbf{y}_i), \forall i \in \{1, \dots, N\}$, be N data points. Let $\mathcal{J}_f(T)$ be the value function in (10). Let $\mathcal{J}_f^\pi(T)$ and $\mathcal{J}_f^\delta(T)$ be numerical implementations of $\mathcal{J}_f(T)$ using a random permutation and a random derangement of \mathbf{y} , respectively. Denote with K the number of points \mathbf{y}_k , with $k \in \{1, \dots, N\}$, in the same position after the permutation (i.e., the fixed points). Then*

$$\mathcal{J}_f^\pi(T) \leq \frac{N-K}{N} \mathcal{J}_f^\delta(T). \quad (20)$$

Lemma 2 practically asserts that the value function $\mathcal{J}_f^\pi(T)$ evaluated via a naive permutation of the data is not a valid variational lower bound of the f -divergence, and thus, there is no guarantee on the optimality of the discriminator's output. In fact, the following theorem states that in the case of the KL divergence, the maximum of $\mathcal{J}_f^\pi(D)$ is attained for a value of the discriminator that is not exactly the density ratio (as it should be from (26), see Sec. A of the Appendix).

Theorem 2. *Let the discriminator $D(\cdot)$ be with enough capacity. Let N be the batch size and f be the generator of the KL divergence. Let $\mathcal{J}_{KL}^\pi(D)$ be defined as*

$$\mathcal{J}_{KL}^\pi(D) = \mathbb{E}_{(\mathbf{x}, \mathbf{y}) \sim p_{XY}(\mathbf{x}, \mathbf{y})} \left[\log \left(D(\mathbf{x}, \mathbf{y}) \right) - f^* \left(\log \left(D(\mathbf{x}, \pi(\mathbf{y})) \right) \right) \right]. \quad (21)$$

Denote with K the number of indices in the same position after the permutation (i.e., the fixed points), and with $R(\mathbf{x}, \mathbf{y})$ the density ratio in (2). Then,

$$\hat{D}(\mathbf{x}, \mathbf{y}) = \arg \max_D \mathcal{J}_{KL}^\pi(D) = \frac{NR(\mathbf{x}, \mathbf{y})}{KR(\mathbf{x}, \mathbf{y}) + N - K}. \quad (22)$$

Although the Theorem is stated for the KL divergence, it can be easily extended to any f -divergence using Theorem 1. Notice that if the number of indices in the same position K is equal to 0, we fall back into the derangement strategy and we retrieve the density ratio as output.

When we parametrize D with a neural network, we perform multiple training iterations and so we have multiple batches of dimension N . This turns into an average analysis on K . We report in the Appendix (see Lemma 5) the proof that, on average, K is equal to 1.

From the previous results, it follows immediately that the estimator obtained using a naive permutation strategy is biased and upper bounded by a function of the batch size N .

Corollary 2.1 (Permutation bound). *Let KL-DIME be the estimator obtained via iterative optimization of $\mathcal{J}_{KL}^\pi(D)$, using a batch of size N every training step. Then,*

$$I_{KL-DIME}^\pi := \mathbb{E}_{(\mathbf{x}, \mathbf{y}) \sim p_{XY}(\mathbf{x}, \mathbf{y})} \left[\log \left(\hat{D}(\mathbf{x}, \mathbf{y}) \right) \right] < \log(N). \quad (23)$$

When specified in the results, we apply the described derangement strategy to train the discriminator using N samples from the joint and N samples from the product of the marginals.

6 Experimental Results

In this section, we first describe the architectures of the proposed estimators. Then, we outline the data used to estimate the MI, and finally comment on the performance of the discussed estimators in different scenarios, also analyzing their computational complexity.

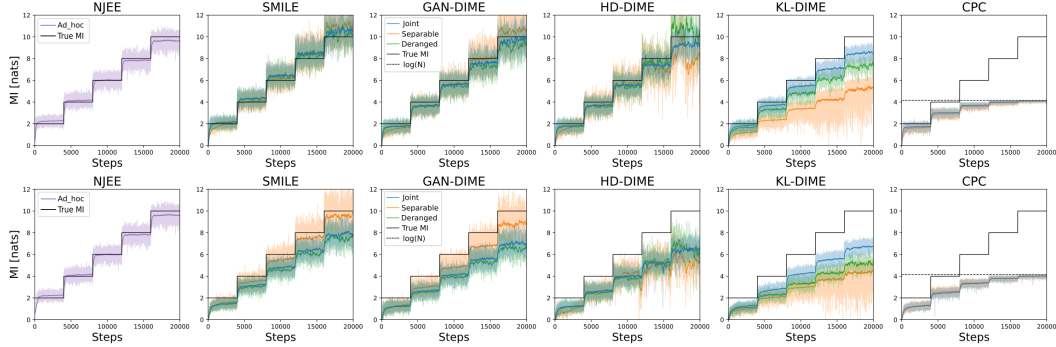


Figure 1: Staircase MI estimation comparison for $d = 20$ and $N = 64$. The *Gaussian* case is reported in the top row, while the *cubic* case is shown in the bottom row.

6.1 Architectures

To demonstrate the behavior of the state-of-the-art MI estimators, we consider multiple neural network *architectures*. The word *architecture* needs to be intended in a wide-sense, meaning that it represents the neural network architecture and its training strategy. In particular, additionally to the architectures **joint** [17] and **separable** [23], we propose the architecture **deranged**.

The **joint** architecture concatenates the samples \mathbf{x} and \mathbf{y} as input of a single neural network. Each training step requires N realizations $(\mathbf{x}_i, \mathbf{y}_i)$ drawn from $p_{XY}(\mathbf{x}, \mathbf{y})$, for $i \in \{1, \dots, N\}$ and $N(N-1)$ samples $(\mathbf{x}_i, \mathbf{y}_j), \forall i, j \in \{1, \dots, N\}$, with $i \neq j$.

The **separable** architecture comprises two neural networks, the former fed in with N realizations of X , the latter with N realizations of Y . The inner product between the outputs of the two networks is exploited to obtain the MI estimate.

The proposed **deranged** architecture feeds a neural network with the concatenation of the samples \mathbf{x} and \mathbf{y} , similarly to the *joint* architecture. However, the *deranged* one obtains the samples of $p_X(\mathbf{x})p_Y(\mathbf{y})$ by performing a derangement of the realizations \mathbf{y} in the batch sampled from $p_{XY}(\mathbf{x}, \mathbf{y})$. Such diverse training strategy solves the main problem of the *joint* architecture: the difficult scalability to large batch sizes. For large values of N , the complexity of the *joint* architecture is $\Omega(N^2)$, while the complexity of the *deranged* one is $\Omega(N)$. NJEE utilizes a specific architecture, in the following referred to as **ad hoc**, comprising $2d - 1$ neural networks, where d is the dimension of X . I_{NJEE} training procedure is supervised: the input of each neural network does not include the \mathbf{y} samples. All the implementation details¹ are reported in Sec. C of the Appendix.

6.2 Multivariate Linear and Nonlinear Gaussians

We benchmark the proposed class of MI estimators on two settings utilized in previous papers [12, 17, 18]. In the first setting (called **Gaussian**), a 20-dimensional Gaussian distribution is sampled to obtain \mathbf{x} and \mathbf{n} samples, independently. Then, \mathbf{y} is obtained as linear combination of \mathbf{x} and \mathbf{n} : $\mathbf{y} = \rho \mathbf{x} + \sqrt{1 - \rho^2} \mathbf{n}$, where ρ is the correlation coefficient. In the second setting (referred to as **cubic**), the nonlinear transformation $\mathbf{y} \mapsto \mathbf{y}^3$ is applied to the Gaussian samples. The true MI follows a staircase shape, where each step is a multiple of 2 *nats*. Each neural network is trained for 4k iterations for each stair step, with a batch size of 64 samples ($N = 64$). The values $d = 20$ and $N = 64$ are used in the literature to compare MI neural estimators. The tested estimators are: I_{NJEE} , $I_{SMILE}(\tau = 1)$, $I_{GAN-DIME}$, $I_{HD-DIME}$, $I_{KL-DIME}$, and I_{CPC} , as illustrated in Fig. 1. The performance of I_{MINE} , I_{NWJ} , and $I_{SMILE}(\tau = \infty)$ is reported in Sec. C of the Appendix, since these algorithms exhibit lower performance compared to both SMILE and *f*-DIME. In fact, all the *f*-DIME estimators have lower variance compared to I_{MINE} , I_{NWJ} , and $I_{SMILE}(\tau = \infty)$, which are characterized by an exponentially increasing variance (see (14)). In particular, all the estimators analyzed belonging to the *f*-DIME class achieve significantly low bias and variance when the true MI is small. Interestingly, for high target MI, different *f*-divergences lead to dissimilar estimation properties. For large MI, $I_{KL-DIME}$ is characterized by a low variance, at the expense of a high bias and a slow rise time. Contrarily, $I_{HD-DIME}$ attains a lower bias at the cost of slightly

¹<https://github.com/tonelloab/fDIME>

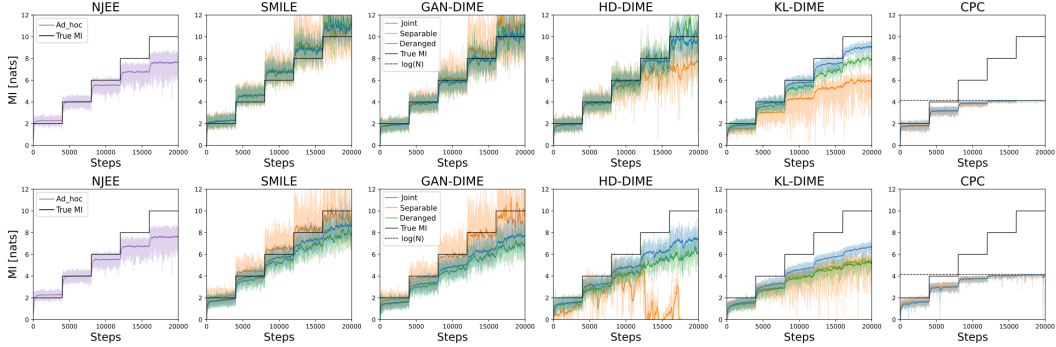


Figure 2: Staircase MI estimation comparison for $d = 5$ and $N = 64$. The *Gaussian* case is reported in the top row, while the *cubic* case is shown in the bottom row.

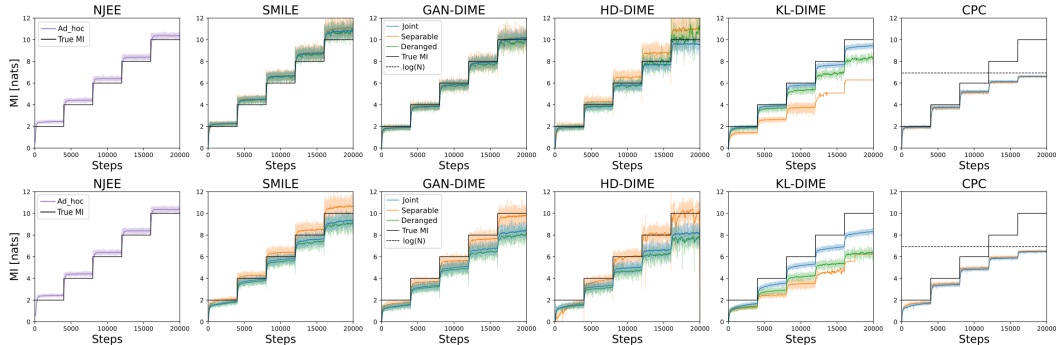


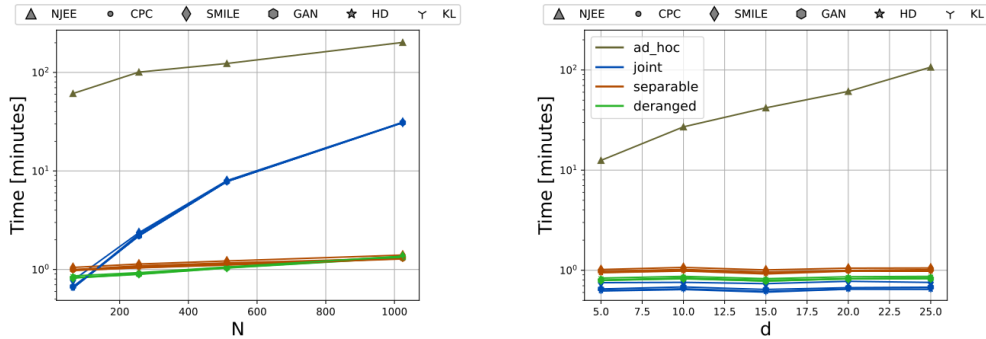
Figure 3: Staircase MI estimation comparison for $d = 20$ and $N = 1024$. The *Gaussian* case is reported in the top row, while the *cubic* case is shown in the bottom row.

higher variance w.r.t. $I_{KL-DIME}$. Diversely, $I_{GAN-DIME}$ achieves the lowest bias, and a variance comparable to $I_{HD-DIME}$.

The MI estimates obtained with I_{SMILE} and $I_{GAN-DIME}$ appear to possess similar behavior, although the value functions of SMILE and GAN-DIME are structurally different. The reason why I_{SMILE} is almost equivalent to $I_{GAN-DIME}$ resides in their training strategy, since they both minimize the same f -divergence. Looking at the implementation code of SMILE², in fact, the network’s training is guided by the gradient computed using the Jensen-Shannon (JS) divergence (a linear transformation of the GAN divergence). Given the trained network, the clipped objective function proposed in [18] is only used to compute the MI estimate, since when (6) is used to train the network, the MI estimate diverges (see Fig. 6 in Sec. C of the Appendix). However, with the proposed class of f -DIME estimators we show that during the estimation phase the partition function (clipped in [18]) is not necessary to obtain the MI estimate.

I_{NJEE} obtains an estimate for $d = 20$ and $N = 64$ that has slightly higher bias than $I_{GAN-DIME}$ for large MI values and slightly higher variance than $I_{KL-DIME}$. I_{CPC} is characterized by high bias and low variance. A schematic comparison between all the MI estimators is reported in Tab. 3 in Sec. C of the Appendix.

When N and d vary, the class of f -DIME estimators proves its robustness (i.e., maintains low bias and variance), as represented in Fig. 2 and 3. Differently, the behavior of I_{CPC} strongly depends on N . At the same time, I_{NJEE} achieves higher bias when N increases and, even more severely, when d decreases (see Fig. 2). Additional results describing all estimators’ behavior when d and N vary are reported and described in Sec. C of the Appendix.



(a) Multivariate Gaussian distribution size fixed to 20. Batch size varying from 64 to 1024.

(b) Multivariate Gaussian distribution size varying from 5 to 25. Batch size fixed to 64.

Figure 4: Time requirements comparison to complete the 5-step staircase MI, for each estimator and each architecture.

Computational Time Analysis

A fundamental characteristic of each algorithm is the computational time. The time requirements to complete the 5-step staircase MI when varying the multivariate Gaussian distribution dimension d and the batch size N are reported in Fig. 4. The difference between I_{SMILE} , I_{CPC} and I_{fDIME} computational time is not significant, when comparing the same architectures. However, as discussed in Sec. 6.1, the *deranged* strategy is significantly faster than the *joint* one as N increases. The fact that the *separable* architecture uses two neural networks implies that when N is significantly large, the *deranged* implementation is much faster than the *separable* one, as well as more stable to the training and distribution parameters, as shown in Sec. C of the Appendix. I_{NJEE} is evaluated with its own architecture, which is the most computationally demanding, because it trains a number of neural networks equal to $2d - 1$. Thus, I_{NJEE} can be utilized only in cases where the time availability is orders of magnitudes higher than the other approaches considered. When d is large, the training of I_{NJEE} fails due to memory requirement problems. For example, our hardware platform (described in Sec. C of the Appendix) does not allow the usage of $d > 30$.

6.3 Self-Consistency Tests

We investigated the three self-consistency tests developed by [18] over images data sets using all the estimators previously described, except I_{NJEE} (for dimension constraints). The f -DIME estimators satisfy two out of the three tests, as discriminative approaches tend to be less precise when the MI is high, in accordance with [18]. Due to space limitations, we report the description of tests and results in Sec. C of the Appendix.

7 Conclusions

In this paper, we presented f -DIME, a class of discriminative mutual information estimators based on the variational representation of the f -divergence. We proved that any valid choice of the function f leads to a low-variance MI estimator which can be parametrized by a neural network. Moreover, we also proposed a derangement training strategy that efficiently samples from the product of marginal distributions. The performance of the class of estimators is evaluated using three functions f , and it is compared with state-of-the-art estimators. Results demonstrate excellent bias/variance trade-off for different data dimensions and different training parameters. The combination of f -DIME with the proposed derangement strategy offers a reliable, efficient and scalable MI estimator.

²<https://github.com/ermongroup/smile-mi-estimator>

References

- [1] Ziv Goldfeld and Kristjan Greenewald. Sliced mutual information: A scalable measure of statistical dependence. *Advances in Neural Information Processing Systems*, 34:17567–17578, 2021.
- [2] Michael Tschannen, Josip Djolonga, Paul K. Rubenstein, Sylvain Gelly, and Mario Lucic. On mutual information maximization for representation learning. In *8th International Conference on Learning Representations, ICLR 2020, Addis Ababa, Ethiopia, April 26-30, 2020*, 2020.
- [3] Dongning Guo, Shlomo Shamai, and Sergio Verdú. Mutual information and minimum mean-square error in gaussian channels. *IEEE transactions on information theory*, 51(4):1261–1282, 2005.
- [4] Josien PW Pluim, JB Antoine Maintz, and Max A Viergever. Mutual-information-based registration of medical images: a survey. *IEEE transactions on medical imaging*, 22(8):986–1004, 2003.
- [5] George Papamakarios, Theo Pavlakou, and Iain Murray. Masked autoregressive flow for density estimation. In *Advances in Neural Information Processing Systems*, volume 30. Curran Associates, Inc., 2017.
- [6] Nunzio A. Letizia and Andrea M. Tonello. Copula density neural estimation. *arXiv preprint arXiv:2211.15353*, 2022.
- [7] Rajat Raina, Yirong Shen, Andrew McCallum, and Andrew Ng. Classification with hybrid generative/discriminative models. *Advances in neural information processing systems*, 16, 2003.
- [8] Andrea M Tonello and Nunzio A Letizia. MIND: Maximum mutual information based neural decoder. *IEEE Communications Letters*, 26(12):2954–2958, 2022.
- [9] David Barber and Felix V. Agakov. The im algorithm: A variational approach to information maximization. In *NIPS*, pages 201–208, 2003.
- [10] Yang Song and Stefano Ermon. Generative modeling by estimating gradients of the data distribution. *Advances in neural information processing systems*, 32, 2019.
- [11] Ian Goodfellow, Jean Pouget-Abadie, Mehdi Mirza, Bing Xu, David Warde-Farley, Sherjil Ozair, Aaron Courville, and Yoshua Bengio. Generative adversarial nets. In *Advances in Neural Information Processing Systems*, volume 27. Curran Associates, Inc., 2014.
- [12] Ben Poole, Sherjil Ozair, Aaron Van Den Oord, Alex Alemi, and George Tucker. On variational bounds of mutual information. In *Proceedings of the 36th International Conference on Machine Learning*, volume 97 of *Proceedings of Machine Learning Research*, pages 5171–5180. PMLR, 09–15 Jun 2019.
- [13] Igal Sason and Sergio Verdú. f -divergence inequalities. *IEEE Transactions on Information Theory*, 62(11):5973–6006, 2016.
- [14] Young-Il Moon, Balaji Rajagopalan, and Upmanu Lall. Estimation of mutual information using kernel density estimators. *Phys. Rev. E*, 52:2318–2321, Sep 1995.
- [15] Alexander Kraskov, Harald Stögbauer, and Peter Grassberger. Estimating mutual information. *Phys. Rev. E*, 69:066138, Jun 2004.
- [16] XuanLong Nguyen, Martin J. Wainwright, and Michael I. Jordan. Estimating divergence functionals and the likelihood ratio by convex risk minimization. *IEEE Transactions on Information Theory*, 56(11):5847–5861, 2010.
- [17] Mohamed Ishmael Belghazi, Aristide Baratin, Sai Rajeshwar, Sherjil Ozair, Yoshua Bengio, Aaron Courville, and Devon Hjelm. Mutual information neural estimation. In *Proceedings of the 35th International Conference on Machine Learning*, volume 80 of *Proceedings of Machine Learning Research*, pages 531–540, Stockholmsmässan, Stockholm Sweden, 10–15 Jul 2018. PMLR.
- [18] Jiaming Song and Stefano Ermon. Understanding the limitations of variational mutual information estimators. In *8th International Conference on Learning Representations, ICLR 2020, Addis Ababa, Ethiopia, April 26-30, 2020*, 2020.
- [19] M. D. Donsker and S. R. S. Varadhan. Asymptotic evaluation of certain markov process expectations for large time. iv. *Communications on Pure and Applied Mathematics*, 36(2):183–212, 1983.

- [20] Aaron van den Oord, Yazhe Li, and Oriol Vinyals. Representation learning with contrastive predictive coding. *arXiv preprint arXiv:1807.03748*, 2018.
- [21] Yuval Shalev, Amichai Painsky, and Irad Ben-Gal. Neural joint entropy estimation. *IEEE Transactions on Neural Networks and Learning Systems*, 2022.
- [22] Sebastian Nowozin, Botond Cseke, and Ryota Tomioka. f-gan: Training generative neural samplers using variational divergence minimization. In D. Lee, M. Sugiyama, U. Luxburg, I. Guyon, and R. Garnett, editors, *Advances in Neural Information Processing Systems*, volume 29. Curran Associates, Inc., 2016.
- [23] Aaron van den Oord, Yazhe Li, and Oriol Vinyals. Representation learning with contrastive predictive coding. *arXiv preprint arXiv:1807.03748*, 2018.
- [24] Subhashis Ghosal, Jayanta K. Ghosh, and Aad W. van der Vaart. Convergence rates of posterior distributions. *The Annals of Statistics*, 28(2):500 – 531, 2000.
- [25] Noga Alon and Joel H Spencer. *The probabilistic method*. John Wiley & Sons, 2016.
- [26] Adam Paszke, Sam Gross, Soumith Chintala, and Gregory Chanan. Pytorch. <https://github.com/pytorch>, 2016.
- [27] Diederik P Kingma and Jimmy Ba. Adam: A method for stochastic optimization. *arXiv preprint arXiv:1412.6980*, 2014.
- [28] Yann LeCun, Léon Bottou, Yoshua Bengio, and Patrick Haffner. Gradient-based learning applied to document recognition. *Proceedings of the IEEE*, 86(11):2278–2324, 1998.
- [29] Han Xiao, Kashif Rasul, and Roland Vollgraf. Fashion-mnist: a novel image dataset for benchmarking machine learning algorithms. *arXiv preprint arXiv:1708.07747*, 2017.

A Appendix A: DIME Estimators

In this section, we provide a concrete list of DIME estimators obtained using three different f -divergences. In particular, we maximize the value function defined in (10)

$$\mathcal{J}_f(T) = \mathbb{E}_{(\mathbf{x}, \mathbf{y}) \sim p_{XY}(\mathbf{x}, \mathbf{y})} \left[T(\mathbf{x}, \mathbf{y}) - f^* \left(T(\mathbf{x}, \sigma(\mathbf{y})) \right) \right],$$

over T or its transformation. By doing that, and using (12),

$$I(X; Y) = I_{fDIME}(X; Y) = \mathbb{E}_{(\mathbf{x}, \mathbf{y}) \sim p_{XY}(\mathbf{x}, \mathbf{y})} \left[\log \left((f^*)'(\hat{T}(\mathbf{x}, \mathbf{y})) \right) \right],$$

we obtain a list of three different MI estimators. The list is used for both commenting on the impact of the f function, referred to as the generator function, and for comparing the estimators discussed in Sec. 2.

We consider the cases when f is the generator of:

- a) the KL divergence;
- b) the GAN divergence;
- c) the Hellinger distance squared.

We report below the derived value functions and the mathematical expressions of the proposed estimators.

A.1 KL divergence

The variational representation of the KL divergence [16] leads to the NWJ estimator in (5) when $f(u) = u \log(u)$. However, since we are interested in extracting the density ratio, we apply the transformation $T(\mathbf{x}) = \log(D(\mathbf{x}))$. In this way, the lower bound introduced in (10) reads as follows

$$\mathcal{J}_{KL}(D) = \mathbb{E}_{(\mathbf{x}, \mathbf{y}) \sim p_{XY}(\mathbf{x}, \mathbf{y})} \left[\log(D(\mathbf{x}, \mathbf{y})) \right] - \mathbb{E}_{(\mathbf{x}, \mathbf{y}) \sim p_X(\mathbf{x})p_Y(\mathbf{y})} \left[D(\mathbf{x}, \mathbf{y}) \right] + 1, \quad (24)$$

which has to be maximized over positive discriminators $D(\cdot)$. As remarked before, we do not use \mathcal{J}_{KL} during the estimation, rather we define the KL-DIME estimator as

$$I_{KL-DIME}(X; Y) := \mathbb{E}_{(\mathbf{x}, \mathbf{y}) \sim p_{XY}(\mathbf{x}, \mathbf{y})} \left[\log \left(\hat{D}(\mathbf{x}, \mathbf{y}) \right) \right], \quad (25)$$

due to the fact that

$$\hat{D}(\mathbf{x}, \mathbf{y}) = \arg \max_D \mathcal{J}_{KL}(D) = \frac{p_{XY}(\mathbf{x}, \mathbf{y})}{p_X(\mathbf{x})p_Y(\mathbf{y})}. \quad (26)$$

A.2 GAN divergence

Following a similar approach, it is possible to define $f(u) = u \log u - (u + 1) \log(u + 1) + \log 4$ and $T(\mathbf{x}) = \log(1 - D(\mathbf{x}))$. We derive from Theorem 1 the GAN-DIME estimator obtained via maximization of

$$\mathcal{J}_{GAN}(D) = \mathbb{E}_{(\mathbf{x}, \mathbf{y}) \sim p_{XY}(\mathbf{x}, \mathbf{y})} \left[\log(1 - D(\mathbf{x}, \mathbf{y})) \right] + \mathbb{E}_{(\mathbf{x}, \mathbf{y}) \sim p_X(\mathbf{x})p_Y(\mathbf{y})} \left[\log(D(\mathbf{x}, \mathbf{y})) \right] + \log(4). \quad (27)$$

In fact, at the equilibrium we recover (3), hence

$$I_{GAN-DIME}(X; Y) := \mathbb{E}_{(\mathbf{x}, \mathbf{y}) \sim p_{XY}(\mathbf{x}, \mathbf{y})} \left[\log \left(\frac{1 - \hat{D}(\mathbf{x}, \mathbf{y})}{\hat{D}(\mathbf{x}, \mathbf{y})} \right) \right]. \quad (28)$$

A.3 Hellinger distance

The last example we consider is the generator of the Hellinger distance squared $f(u) = (\sqrt{u} - 1)^2$ with the change of variable $T(\mathbf{x}) = 1 - D(\mathbf{x})$. After simple manipulations, we obtain the associated value function as

$$\mathcal{J}_{HD}(D) = 2 - \mathbb{E}_{(\mathbf{x}, \mathbf{y}) \sim p_{XY}(\mathbf{x}, \mathbf{y})} \left[D(\mathbf{x}, \mathbf{y}) \right] - \mathbb{E}_{(\mathbf{x}, \mathbf{y}) \sim p_X(\mathbf{x})p_Y(\mathbf{y})} \left[\frac{1}{D(\mathbf{x}, \mathbf{y})} \right], \quad (29)$$

which is maximized for

$$\hat{D}(\mathbf{x}, \mathbf{y}) = \arg \max_D \mathcal{J}_{HD}(D) = \sqrt{\frac{p_X(\mathbf{x})p_Y(\mathbf{y})}{p_{XY}(\mathbf{x}, \mathbf{y})}}, \quad (30)$$

leading to the HD-DIME estimator

$$I_{HD-DIME}(X; Y) := \mathbb{E}_{(\mathbf{x}, \mathbf{y}) \sim p_{XY}(\mathbf{x}, \mathbf{y})} \left[\log \left(\frac{1}{\hat{D}^2(\mathbf{x}, \mathbf{y})} \right) \right]. \quad (31)$$

Given that these estimators comprise only one expectation over the joint samples, their variance has different properties compared to the variational ones requiring the partition term such as MINE and NWJ.

B Appendix B: Proofs of Lemmas and Theorems

B.1 Proof of Theorem 1

Theorem 1. *Let $(X, Y) \sim p_{XY}(\mathbf{x}, \mathbf{y})$ be a pair of random variables. Let $\sigma(\cdot)$ be a permutation function such that $p_{\sigma(Y)}(\sigma(\mathbf{y})|\mathbf{x}) = p_Y(\mathbf{y})$. Let f^* be the Fenchel conjugate of $f : \mathbb{R}_+ \rightarrow \mathbb{R}$, a convex lower semicontinuous function that satisfies $f(1) = 0$ with derivative f' . If $\mathcal{J}_f(T)$ is a value function defined as*

$$\mathcal{J}_f(T) = \mathbb{E}_{(\mathbf{x}, \mathbf{y}) \sim p_{XY}(\mathbf{x}, \mathbf{y})} \left[T(\mathbf{x}, \mathbf{y}) - f^* \left(T(\mathbf{x}, \sigma(\mathbf{y})) \right) \right], \quad (32)$$

then

$$\hat{T}(\mathbf{x}, \mathbf{y}) = \arg \max_T \mathcal{J}_f(T) = f' \left(\frac{p_{XY}(\mathbf{x}, \mathbf{y})}{p_X(\mathbf{x})p_Y(\mathbf{y})} \right), \quad (33)$$

and

$$I(X; Y) = I_{fDIME}(X; Y) = \mathbb{E}_{(\mathbf{x}, \mathbf{y}) \sim p_{XY}(\mathbf{x}, \mathbf{y})} \left[\log \left((f^*)'(\hat{T}(\mathbf{x}, \mathbf{y})) \right) \right]. \quad (34)$$

Proof. From the hypothesis, the value function can be rewritten as

$$\mathcal{J}_f(T) = \mathbb{E}_{(\mathbf{x}, \mathbf{y}) \sim p_{XY}(\mathbf{x}, \mathbf{y})} \left[T(\mathbf{x}, \mathbf{y}) \right] - \mathbb{E}_{(\mathbf{x}, \mathbf{y}) \sim p_X(\mathbf{x})p_Y(\mathbf{y})} \left[f^* \left(T(\mathbf{x}, \mathbf{y}) \right) \right]. \quad (35)$$

The thesis follows immediately from Lemma 1 of [16]. Indeed, the f -divergence D_f can be expressed in terms of its lower bound via Fenchel convex duality

$$D_f(P||Q) \geq \sup_{T \in \mathbb{R}} \left\{ \mathbb{E}_{x \sim p(x)} [T(x)] - \mathbb{E}_{x \sim q(x)} [f^*(T(x))] \right\}, \quad (36)$$

where $T : \mathcal{X} \rightarrow \mathbb{R}$ and f^* is the Fenchel conjugate of f defined as

$$f^*(t) := \sup_{u \in \mathbb{R}} \{ut - f(u)\}. \quad (37)$$

Therein, it was shown that the bound in (36) is tight for optimal values of $T(x)$ and it takes the following form

$$\hat{T}(x) = f' \left(\frac{p(x)}{q(x)} \right), \quad (38)$$

where f' is the derivative of f .

The mutual information $I(X; Y)$ admits the KL divergence representation

$$I(X; Y) = D_{KL}(p_{XY} || p_X p_Y), \quad (39)$$

and since the inverse of the derivative of f is the derivative of the conjugate f^* , the density ratio can be rewritten in terms of the optimum discriminator \hat{T}

$$(f')^{-1}(\hat{T}(\mathbf{x}, \mathbf{y})) = (f^*)'(\hat{T}(\mathbf{x}, \mathbf{y})) = \frac{p_{XY}(\mathbf{x}, \mathbf{y})}{p_X(\mathbf{x})p_Y(\mathbf{y})}. \quad (40)$$

f -DIME finally reads as follows

$$I_{fDIME}(X; Y) = \mathbb{E}_{(x, y) \sim p_{XY}(\mathbf{x}, \mathbf{y})} \left[\log \left((f^*)'(\hat{T}(\mathbf{x}, \mathbf{y})) \right) \right]. \quad (41)$$

□

B.2 Proof of Lemma 1

Lemma 1. Let $\hat{R} = p_{XY}(\mathbf{x}, \mathbf{y}) / (p_X(\mathbf{x})p_Y(\mathbf{y}))$ and assume $\text{Var}_{p_{XY}}[\log \hat{R}]$ exists. Let p_{XY}^M be the empirical distribution of M i.i.d. samples from p_{XY} and let $\mathbb{E}_{p_{XY}^M}$ denote the sample average over p_{XY}^M . Then, under the randomness of the sampling procedure, it holds that

$$\text{Var}_{p_{XY}} [\mathbb{E}_{p_{XY}^M} [\log \hat{R}]] \leq \frac{4H^2(p_{XY}, p_X p_Y) \|\hat{R}\|_\infty - I^2(X; Y)}{M} \quad (42)$$

where H^2 is the Hellinger distance squared defined as

$$H^2(p, q) = \int_{\mathbf{x}} \left(\sqrt{p(\mathbf{x})} - \sqrt{q(\mathbf{x})} \right)^2 d\mathbf{x}, \quad (43)$$

and the infinity norm is defined as $\|f(x)\|_\infty := \sup_{x \in \mathbb{R}} |f(x)|$.

Proof. Consider the variance of $\hat{R}(\mathbf{x}, \mathbf{y})$ when $(\mathbf{x}, \mathbf{y}) \sim p_{XY}(\mathbf{x}, \mathbf{y})$, then

$$\text{Var}_{p_{XY}} [\log \hat{R}] = \mathbb{E}_{p_{XY}} \left[\left(\log \frac{p_{XY}}{p_X p_Y} \right)^2 \right] - \left(\mathbb{E}_{p_{XY}} \left[\log \frac{p_{XY}}{p_X p_Y} \right] \right)^2. \quad (44)$$

The power of the log-density ratio is upper bounded as follows (see the approach of Lemma 8.3 in [24])

$$\mathbb{E}_{p_{XY}} \left[\left(\log \frac{p_{XY}}{p_X p_Y} \right)^2 \right] \leq 4H^2(p_{XY}, p_X p_Y) \left\| \frac{p_{XY}}{p_X p_Y} \right\|_\infty, \quad (45)$$

while the mean squared is the ground-truth mutual information squared, thus

$$\text{Var}_{p_{XY}} [\log \hat{R}] \leq 4H^2(p_{XY}, p_X p_Y) \left\| \frac{p_{XY}}{p_X p_Y} \right\|_\infty - I^2(X; Y). \quad (46)$$

Finally, the variance of the mean of M i.i.d. random variables yields the thesis

$$\text{Var}_{p_{XY}} [\mathbb{E}_{p_{XY}^M} [\log \hat{R}]] = \frac{\text{Var}_{p_{XY}} [\log \hat{R}]}{M} \leq \frac{4H^2(p_{XY}, p_X p_Y) \left\| \frac{p_{XY}}{p_X p_Y} \right\|_\infty - I^2(X; Y)}{M}. \quad (47)$$

□

B.3 Proof of Lemma 2

Lemma 2. Let $(\mathbf{x}_i, \mathbf{y}_i), \forall i \in \{1, \dots, N\}$, be N data points. Let $\mathcal{J}_f(T)$ be the value function in (10). Let $\mathcal{J}_f^\pi(T)$ and $\mathcal{J}_f^\delta(T)$ be numerical implementations of $\mathcal{J}_f(T)$ using a random permutation and a random derangement of \mathbf{y} , respectively. Denote with K the number of points \mathbf{y}_k , with $k \in \{1, \dots, N\}$, in the same position after the permutation (i.e., the fixed points). Then

$$\mathcal{J}_f^\pi(T) \leq \frac{N-K}{N} \mathcal{J}_f^\delta(T). \quad (48)$$

Proof. Define $\mathcal{J}_f^\pi(T)$ as the Monte Carlo implementation of $\mathcal{J}_f(T)$ when using the permutation function $\pi(\cdot)$

$$\mathcal{J}_f^\pi(T) = \frac{1}{N} \sum_{i=1}^N T(\mathbf{x}_i, \mathbf{y}_i) - \frac{1}{N} \sum_{i=1}^N f^*(T(\mathbf{x}_i, \mathbf{y}_j)), \quad (49)$$

where the pair $(\mathbf{x}_i, \mathbf{y}_j)$ is obtained via a random permutation of the elements of \mathbf{y} as $j = \pi(i)$, $\forall i \in \{1, \dots, N\}$. Since K is a non-negative integer representing the number of fixed points $i = \pi(i)$, the value function can be rewritten as

$$\mathcal{J}_f^\pi(T) = \frac{1}{N} \sum_{i=1}^N T(\mathbf{x}_i, \mathbf{y}_i) - \frac{1}{N} \sum_{i=1}^K f^*(T(\mathbf{x}_i, \mathbf{y}_i)) - \frac{1}{N} \sum_{i=1}^{N-K} f^*(T(\mathbf{x}_i, \mathbf{y}_{j \neq i})), \quad (50)$$

which can also be expressed as

$$\mathcal{J}_f^\pi(T) = \frac{1}{N} \sum_{i=1}^K T(\mathbf{x}_i, \mathbf{y}_i) + \frac{1}{N} \sum_{i=1}^{N-K} T(\mathbf{x}_i, \mathbf{y}_i) - \frac{1}{N} \sum_{i=1}^K f^*(T(\mathbf{x}_i, \mathbf{y}_i)) - \frac{1}{N} \sum_{i=1}^{N-K} f^*(T(\mathbf{x}_i, \mathbf{y}_{j \neq i})). \quad (51)$$

In (51) it is possible to recognize that the second and last term of the RHS constitutes the numerical implementation of $\mathcal{J}_f(T)$ using a derangement strategy on $N - K$ elements, so that

$$\mathcal{J}_f^\pi(T) = \frac{1}{N} \sum_{i=1}^K T(\mathbf{x}_i, \mathbf{y}_i) - \frac{1}{N} \sum_{i=1}^K f^*(T(\mathbf{x}_i, \mathbf{y}_i)) + \frac{N-K}{N} \mathcal{J}_f^\delta(T). \quad (52)$$

However, by definition of Fenchel conjugate

$$\frac{1}{N} \sum_{i=1}^K T(\mathbf{x}_i, \mathbf{y}_i) - f^*(T(\mathbf{x}_i, \mathbf{y}_i)) \leq 0, \quad (53)$$

since for $t = 1$

$$u - f^*(u) \leq u - (ut - f(t)) = f(1) = 0. \quad (54)$$

Hence, we can conclude that

$$\mathcal{J}_f^\pi(T) \leq \frac{N-K}{N} \mathcal{J}_f^\delta(T). \quad (55)$$

□

B.4 Proof of Theorem 2

Theorem 2. Let the discriminator $D(\cdot)$ be with enough capacity. Let N be the batch size and f be the generator of the KL divergence. Let $\mathcal{J}_{KL}^\pi(D)$ be defined as

$$\mathcal{J}_{KL}^\pi(D) = \mathbb{E}_{(\mathbf{x}, \mathbf{y}) \sim p_{\mathbf{X}\mathbf{Y}}(\mathbf{x}, \mathbf{y})} \left[\log \left(D(\mathbf{x}, \mathbf{y}) \right) - f^* \left(\log \left(D(\mathbf{x}, \pi(\mathbf{y})) \right) \right) \right]. \quad (56)$$

Denote with K the number of indices in the same position after the permutation (i.e., the fixed points), and with $R(\mathbf{x}, \mathbf{y})$ the density ratio in (2). Then,

$$\hat{D}(\mathbf{x}, \mathbf{y}) = \arg \max_D \mathcal{J}_{KL}^\pi(D) = \frac{NR(\mathbf{x}, \mathbf{y})}{KR(\mathbf{x}, \mathbf{y}) + N - K}. \quad (57)$$

Proof. The idea of the proof is to express $\mathcal{J}_{KL}^\pi(D)$ via Monte Carlo approximation, in order to rearrange fixed points, and then go back to Lebesgue integration. The value function $\mathcal{J}_{KL}(D)$ can be written as

$$\mathcal{J}_{KL}(D) = \mathbb{E}_{(\mathbf{x}, \mathbf{y}) \sim p_{XY}(\mathbf{x}, \mathbf{y})} \left[\log(D(\mathbf{x}, \mathbf{y})) \right] - \mathbb{E}_{(\mathbf{x}, \mathbf{y}) \sim p_X(\mathbf{x})p_Y(\mathbf{y})} \left[D(\mathbf{x}, \mathbf{y}) \right] + 1. \quad (58)$$

Similarly to (50), we can express $\mathcal{J}_{KL}^\pi(D)$ as

$$\mathcal{J}_{KL}^\pi(D) = \frac{1}{N} \sum_{i=1}^N \log(D(\mathbf{x}_i, \mathbf{y}_i)) - \frac{1}{N} \sum_{i=1}^K D(\mathbf{x}_i, \mathbf{y}_i) - \frac{1}{N} \sum_{i=1}^{N-K} D(\mathbf{x}_i, \mathbf{y}_{j \neq i}) + 1, \quad (59)$$

where K is the number of fixed points of the permutation $j = \pi(i), \forall i \in \{1, \dots, N\}$. However, when $N \rightarrow \infty$, we can use Lebesgue integration and rewrite (59) as

$$\begin{aligned} \mathcal{J}_{KL}^\pi(D) &= \int_{\mathbf{x}} \int_{\mathbf{y}} \left(p_{XY}(\mathbf{x}, \mathbf{y}) \log(D(\mathbf{x}, \mathbf{y})) - \frac{K}{N} p_{XY}(\mathbf{x}, \mathbf{y}) D(\mathbf{x}, \mathbf{y}) \right) d\mathbf{x} d\mathbf{y} \\ &\quad - \int_{\mathbf{x}} \int_{\mathbf{y}} \frac{N-K}{N} p_X(\mathbf{x}) p_Y(\mathbf{y}) D(\mathbf{x}, \mathbf{y}) d\mathbf{x} d\mathbf{y} + 1. \end{aligned} \quad (60)$$

To maximize $\mathcal{J}_{KL}^\pi(D)$, it is enough to take the derivative of the integrand with respect to D and equate it to 0, yielding the following equation in D

$$\frac{p_{XY}(\mathbf{x}, \mathbf{y})}{D(\mathbf{x}, \mathbf{y})} - \frac{K}{N} p_{XY}(\mathbf{x}, \mathbf{y}) - \frac{N-K}{N} p_X(\mathbf{x}) p_Y(\mathbf{y}) = 0. \quad (61)$$

Solving for D leads to the thesis

$$\hat{D}(\mathbf{x}, \mathbf{y}) = \frac{NR(\mathbf{x}, \mathbf{y})}{KR(\mathbf{x}, \mathbf{y}) + N - K}, \quad (62)$$

since $\mathcal{J}_{KL}^\pi(\hat{D})$ is a maximum being the second derivative w.r.t. D a non-positive function. \square

B.5 Proof of Corollary 2.1

Corollary 2.1 (Permutation bound). *Let KL-DIME be the estimator obtained via iterative optimization of $\mathcal{J}_{KL}^\pi(D)$, using a batch of size N every training step. Then,*

$$I_{KL-DIME}^\pi := \mathbb{E}_{(\mathbf{x}, \mathbf{y}) \sim p_{XY}(\mathbf{x}, \mathbf{y})} \left[\log \left(\hat{D}(\mathbf{x}, \mathbf{y}) \right) \right] < \log(N). \quad (63)$$

Proof. Theorem 2 implies that, when the batch size is much larger than the density ratio ($N \gg R$), then the discriminator's output converges to the density ratio. Indeed,

$$\lim_{N \rightarrow \infty} \hat{D}(\mathbf{x}, \mathbf{y}) = \lim_{N \rightarrow \infty} \frac{NR(\mathbf{x}, \mathbf{y})}{KR(\mathbf{x}, \mathbf{y}) + N - K} = R(\mathbf{x}, \mathbf{y}). \quad (64)$$

Instead, when the density ratio is much larger than the batch size ($R \gg N$), then the discriminator's output converges to a constant, in particular

$$\lim_{R \rightarrow \infty} \hat{D}(\mathbf{x}, \mathbf{y}) = \lim_{R \rightarrow \infty} \frac{NR(\mathbf{x}, \mathbf{y})}{KR(\mathbf{x}, \mathbf{y}) + N - K} = \frac{N}{K}. \quad (65)$$

However, from Lemma 5, it is true that $K = 1$ on average. Therefore, an iterative optimization algorithm leads to an upper-bounded discriminator, since

$$\hat{D}(\mathbf{x}, \mathbf{y}) < N, \quad (66)$$

which implies the thesis. \square

B.6 Proof of Lemma 3

Lemma 3. *Let the discriminator $T(\cdot)$ be with enough capacity, i.e., in the non parametric limit. Consider the problem*

$$\hat{T} = \arg \max_T \mathcal{J}_f(T) \quad (67)$$

where

$$\mathcal{J}_f(T) = \mathbb{E}_{(\mathbf{x}, \mathbf{y}) \sim p_{XY}(\mathbf{x}, \mathbf{y})} \left[T(\mathbf{x}, \mathbf{y}) \right] - \mathbb{E}_{(\mathbf{x}, \mathbf{y}) \sim p_X(\mathbf{x})p_Y(\mathbf{y})} \left[f^* \left(T(\mathbf{x}, \mathbf{y}) \right) \right]. \quad (68)$$

and the update rule based on the gradient descent method

$$T^{(n+1)} = T^{(n)} + \mu \nabla \mathcal{J}_f(T^{(n)}). \quad (69)$$

If the gradient descent method converges to the global optimum \hat{T} , the mutual information estimator

$$I(X; Y) = I_{fDIME}(X; Y) = \mathbb{E}_{(\mathbf{x}, \mathbf{y}) \sim p_{XY}(\mathbf{x}, \mathbf{y})} \left[\log \left((f^*)'(\hat{T}(\mathbf{x}, \mathbf{y})) \right) \right]. \quad (70)$$

converges to the real value of the mutual information $I(X; Y)$.

Proof. For convenience of notation, let the instantaneous mutual information be the random variable defined as

$$i(X; Y) := \log \left(\frac{p_{XY}(\mathbf{x}, \mathbf{y})}{p_X(\mathbf{x})p_Y(\mathbf{y})} \right). \quad (71)$$

It is straightforward to notice that the MI corresponds to the expected value of $i(X; Y)$ over the joint distribution p_{XY} . The solution to (67) is given by (11) of Theorem 1. Let $\delta^{(n)} = \hat{T} - T^{(n)}$ be the displacement between the optimum discriminator \hat{T} and the obtained one $T^{(n)}$ at the iteration n , then

$$\hat{i}_{n, fDIME}(X; Y) = \log \left((f^*)'(T^{(n)}(\mathbf{x}, \mathbf{y})) \right) = \log \left(R^{(n)}(\mathbf{x}, \mathbf{y}) \right), \quad (72)$$

where $R^{(n)}(\mathbf{x}, \mathbf{y})$ represents the estimated density ratio at the n -th iteration and it is related with the optimum ratio $\hat{R}(\mathbf{x}, \mathbf{y})$ as follows

$$\begin{aligned} \hat{R} - R^{(n)} &= (f^*)'(\hat{T}) - (f^*)'(T^{(n)}) \\ &= (f^*)'(\hat{T}) - (f^*)'(\hat{T} - \delta^{(n)}) \\ &\simeq \delta^{(n)} \cdot \left[(f^*)''(\hat{T} - \delta^{(n)}) \right], \end{aligned} \quad (73)$$

where the last step follows from a first order Taylor expansion in $\hat{T} - \delta^{(n)}$. Therefore,

$$\begin{aligned} \hat{i}_{n, fDIME}(X; Y) &= \log(R^{(n)}) \\ &= \log \left((\hat{R}) \left(1 - \delta^{(n)} \cdot \frac{(f^*)''(\hat{T} - \delta^{(n)})}{(f^*)'(\hat{T})} \right) \right) \\ &= i(X; Y) + \log \left(1 - \delta^{(n)} \cdot \frac{(f^*)''(\hat{T} - \delta^{(n)})}{(f^*)'(\hat{T})} \right). \end{aligned} \quad (74)$$

If the gradient descent method converges towards the optimum solution \hat{T} , $\delta^{(n)} \rightarrow 0$ and

$$\begin{aligned} \hat{i}_{n, fDIME}(X; Y) &\simeq i(X; Y) - \delta^{(n)} \cdot \left[\frac{(f^*)''(\hat{T} - \delta^{(n)})}{(f^*)'(\hat{T})} \right] \\ &\simeq i(X; Y) - \delta^{(n)} \cdot \left[\frac{(f^*)''(\hat{T})}{(f^*)'(\hat{T})} \right] \\ &= i(X; Y) - \delta^{(n)} \cdot \left[\frac{d}{dT} \log((f^*)'(T)) \Big|_{T=\hat{T}} \right], \end{aligned} \quad (75)$$

where the RHS is itself a first order Taylor expansion of the instantaneous mutual information in \hat{T} . In the asymptotic limit ($n \rightarrow +\infty$), it holds also for the expected values that

$$|I(X; Y) - \hat{I}_{n, fDIME}(X; Y)| \rightarrow 0. \quad (76)$$

□

B.7 Proof of Lemma 4

Lemma 4. *Let \hat{R} be the optimal density ratio and let $X \sim \mathcal{N}(0, \sigma_X^2)$ and $N \sim \mathcal{N}(0, \sigma_N^2)$ be uncorrelated scalar Gaussian random variables such that $Y = X + N$. Assume $\text{Var}_{p_{XY}}[\log \hat{R}]$ exists. Let p_{XY}^M be the empirical distribution of M i.i.d. samples from p_{XY} and let $\mathbb{E}_{p_{XY}^M}$ denote the sample average over p_{XY}^M . Then, under the randomness of the sampling procedure, it holds that*

$$\text{Var}_{p_{XY}}[\mathbb{E}_{p_{XY}^M}[\log \hat{R}]] = \frac{1 - e^{-2I(X; Y)}}{M}. \quad (77)$$

Proof. From the hypothesis, the density ratio can be rewritten as $\hat{R} = p_N(y - x)/p_Y(y)$ and the output variance is clearly equal to $\sigma_Y^2 = \sigma_X^2 + \sigma_N^2$. Notice that this is equivalent of having correlated random variables X and Y with correlation coefficient ρ , since it is enough to study the case $\sigma_X = \rho$ and $\sigma_N = \sqrt{1 - \rho^2}$.

It is easy to verify via simple calculations that

$$\begin{aligned} I(X; Y) &= \mathbb{E}_{p_{XY}}[\log \hat{R}] \\ &= \log \frac{\sigma_Y}{\sigma_N} + \mathbb{E}_{p_{XY}} \left[\frac{y^2}{2\sigma_Y^2} - \frac{(y-x)^2}{2\sigma_N^2} \right] \\ &= \dots = \log \frac{\sigma_Y}{\sigma_N} = \frac{1}{2} \log \left(1 + \frac{\sigma_X^2}{\sigma_N^2} \right) = -\frac{1}{2} \log(1 - \rho^2). \end{aligned} \quad (78)$$

Similarly,

$$\begin{aligned} \text{Var}_{p_{XY}}[\log \hat{R}] &= \mathbb{E}_{p_{XY}} \left[\left(\log \left(\frac{\sigma_Y}{\sigma_N} \right) + \frac{y^2}{2\sigma_Y^2} - \frac{(y-x)^2}{2\sigma_N^2} \right)^2 \right] - I^2(X; Y) \\ &= \frac{1}{4} \mathbb{E}_{p_{XY}} \left[\left(\frac{y-x}{\sigma_N} \right)^4 + \left(\frac{y}{\sigma_Y} \right)^4 - 2 \left(\frac{y}{\sigma_Y} \right)^2 \left(\frac{y-x}{\sigma_N} \right)^2 \right] \\ &= \dots = \text{Kurt}[Z] \left(\frac{1}{2} - \frac{\sigma_N^2}{2\sigma_Y^2} \right) - \frac{\sigma_X^2}{2\sigma_Y^2} \\ &= \frac{\sigma_X^2}{\sigma_Y^2} = 1 - \frac{\sigma_N^2}{\sigma_Y^2} = 1 - e^{-2I(X; Y)} = \rho^2, \end{aligned} \quad (79)$$

where the last steps use the fact that the Kurtosis of a normal distribution is 3 and that the mutual information can be expressed as in (78). Finally, the variance of the mean of M i.i.d. random variables yields the thesis

$$\text{Var}_{p_{XY}}[\mathbb{E}_{p_{XY}^M}[\log \hat{R}]] = \frac{\text{Var}_{p_{XY}}[\log \hat{R}]}{M}. \quad (80)$$

If X and N are multivariate Gaussians with diagonal covariance matrices $\rho^2 \mathbb{I}_{d \times d}$ and $(1 - \rho^2) \mathbb{I}_{d \times d}$, the results for both the MI and variance in the scalar case are simply multiplied by d . □

B.8 Proof of Lemma 5

Lemma 5 (see [25]). *The average number of fixed points in a random permutation $\pi(\cdot)$ is equal to 1.*

Proof. Let $\pi(\cdot)$ be a random permutation on $\{1, \dots, N\}$. Let the random variable X represent the number of fixed points (i.e., the number of cycles of length 1) of $\pi(\cdot)$. We define $X = X_1 + X_2 +$

$\dots + X_N$, where $X_i = 1$ when $\pi(i) = i$, and 0 otherwise. $\mathbb{E}[X]$ is computed by exploiting the linearity property of expectation. Trivially,

$$\mathbb{E}[X_i] = \mathbb{P}[\pi(i) = i] = \frac{1}{N}, \quad (81)$$

which implies

$$\mathbb{E}[X] = \sum_{i=1}^N \frac{1}{N} = 1. \quad (82)$$

□

C Appendix C: Experimental Details

C.1 Multivariate Linear and Nonlinear Gaussians Experiments

The neural network architectures implemented for the linear and cubic Gaussian experiments are: *joint*, *separable*, *deranged*, and the architecture of NJEE, referred to as *ad hoc*.

Joint architecture. The *joint* architecture is a feed-forward fully connected neural network with an input size equal to twice the dimension of the samples distribution ($2d$), one output neuron, and two hidden layers of 256 neurons each. The activation function utilized in each layer (except from the last one) is ReLU. The number of realizations (\mathbf{x}, \mathbf{y}) fed as input of the neural network for each training iteration is N^2 , obtained as all the combinations of the samples \mathbf{x} and \mathbf{y} drawn from $p_{XY}(\mathbf{x}, \mathbf{y})$.

Separable architecture. The *separable* architecture comprises two feed-forward neural networks, each one with an input size equal to d , output layer containing 32 neurons and 2 hidden layers with 256 neurons each. The ReLU activation function is used in each layer (except from the last one). The first network is fed in with N realizations of X , while the second one with N realizations of Y .

Deranged architecture. The *deranged* architecture is a feed-forward fully connected neural network with an input size equal to twice the dimension of the samples distribution ($2d$), one output neuron, and two hidden layers of 256 neurons each. The activation function utilized in each layer (except from the last one) is ReLU. The number of realizations (\mathbf{x}, \mathbf{y}) the neural network is fed with is $2N$ for each training iteration: N realizations drawn from $p_{XY}(\mathbf{x}, \mathbf{y})$ and N realizations drawn from $p_X(\mathbf{x})p_Y(\mathbf{y})$ using the derangement procedure described in Sec. 5.

The architecture *deranged* is not used for I_{CPC} because in (7) the summation at the denominator of the argument of the logarithm would require neural network predictions corresponding to the inputs $(\mathbf{x}_i, \mathbf{y}_j)$, $\forall i, j \in \{1, \dots, N\}$ with $i \neq j$.

Ad hoc architecture. The *NJEE* MI estimator comprises $2d - 1$ feed-forward neural networks. Each neural network is composed by an input layer with size between 1 and $2d - 1$, an output layer containing $N - k$ neurons, with $k \in \mathbb{N}$ small, and 2 hidden layers with 256 neurons each. The ReLU activation function is used in each layer (except from the last one). We implemented a Pytorch [26] version of the code produced by the authors of [21]³, to unify NJEE with all the other MI estimators.

Each neural estimator is trained using Adam optimizer [27], with learning rate 5×10^{-4} , $\beta_1 = 0.9$, $\beta_2 = 0.999$. The batch size is initially set to $N = 64$.

For the *Gaussian* setting, we sample a 20-dimensional Gaussian distribution to obtain \mathbf{x} and \mathbf{n} samples, independently. Then, we compute \mathbf{y} as linear combination of \mathbf{x} and \mathbf{n} : $\mathbf{y} = \rho \mathbf{x} + \sqrt{1 - \rho^2} \mathbf{n}$, where ρ is the correlation coefficient. For the *cubic* setting, the nonlinear transformation $\mathbf{y} \mapsto \mathbf{y}^3$ is applied to the Gaussian samples. During the training procedure, every $4k$ iterations, the target value of the MI is increased by 2 nats , for 5 times, obtaining a target staircase with 5 steps. The change in target MI is obtained by increasing ρ , that affects the true MI according to

$$I(X; Y) = -\frac{d}{2} \log(1 - \rho^2). \quad (83)$$

C.1.1 Supplementary Analysis of the MI Estimators Performance

Additional plots reporting the MI estimates obtained from MINE, NWJ, and SMILE with $\tau = \infty$, are outlined in Fig. 5. The variance attained by these algorithms exponentially increases as the true MI grows, as stated in (14).

³<https://github.com/YuvalShalev/NJEE>

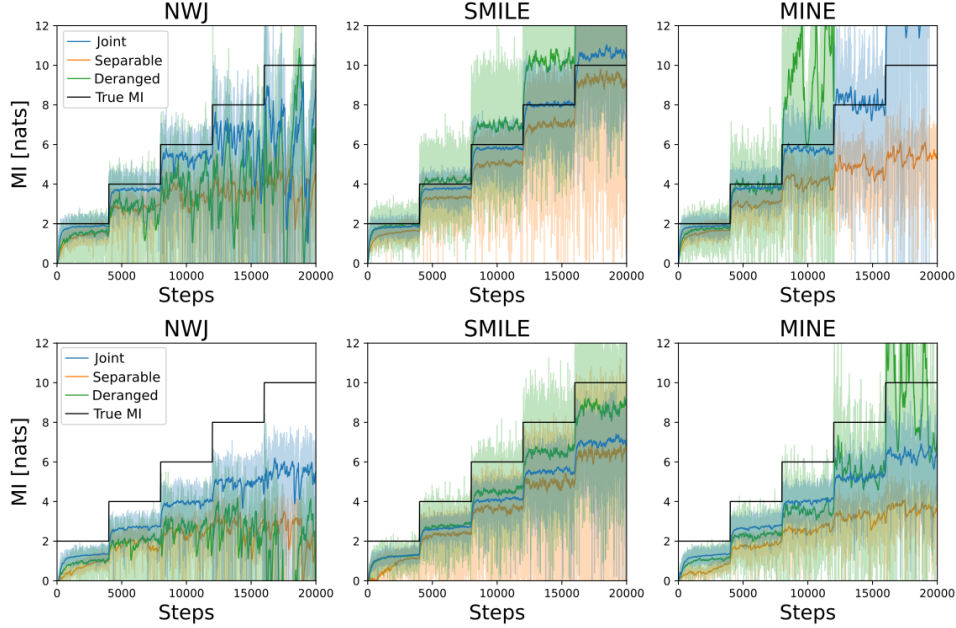


Figure 5: NWJ, SMILE ($\tau = \infty$), and MINE MI estimation comparison with $d = 20$ and $N = 64$. The *Gaussian* setting is represented in the top row, while the *cubic* setting is shown in the bottom row.

We report in Fig. 6 the behavior we obtained for I_{SMILE} when the training of the neural network is performed by using the cost function in (6). The training diverges during the first steps when $\tau = 1$ and $\tau = 5$. Differently, when $\tau = \infty$, I_{SMILE} corresponds to I_{MINE} (without the moving average improvement), therefore the MI estimate does not diverge. Interestingly, by comparing I_{SMILE} ($\tau = \infty$) trained with the JS divergence and with the MINE cost function (in Fig. 5 and Fig. 6, respectively), the variance of the latter case is significantly higher. Hence, the JS maximization trick seems to have an impact in lowering the estimator variance.

C.1.2 Analysis for Different Values of d and N

The class of f -DIME estimators is robust to changes in d and N , as the estimators' variance decreases (see (77) and Fig. 10) when N increases and their achieved bias is not significantly influenced by the choice of d . Differently, I_{NJEE} and I_{CPC} are highly affected by variations of those parameters, as described in Fig. 2 and Fig. 3. More precisely, I_{CPC} is not strongly influenced by a change of d , but the bias significantly increases as the batch size diminishes, since the upper bound lowers. I_{NJEE} achieves a higher bias both when d decreases and when N increases w.r.t. the default values $d = 20$, $N = 64$. In addition, when d is large, the training of I_{NJEE} is not feasible, as it requires a lot of time (see Fig. 4) and memory (as a consequence of the large number of neural networks utilized) requirements.

We show the achieved bias, variance, and mean squared error (MSE) corresponding to the three settings reported in Fig. 1, 2, and 3 in Fig. 7, 8, and 9, respectively. The achieved variance is bounded when the estimator used is $I_{KL-DIME}$ or I_{CPC} . In particular, Figures 7, 8, 9, and 10 demonstrate that $I_{KL-DIME}$ satisfies Lemma 4.

Additionally, we report the achieved bias, variance and MSE when $d = 20$ and N varies according to Tab. 1. We use the notation $N = [512, 1024]$ to indicate that each cell of the table reports the values corresponding to $N = 512$ and $N = 1024$, with this specific order, inside the brackets. Similarly, we show the attained bias, variance, and MSE for $d = [5, 10]$ and $N = 64$ in Tab. 2. The achieved bias, variance and MSE shown in Tab. 1 and Tab. 2 motivate that the class of f -dime estimators attains the best values for bias and MSE. Similarly, $I_{KL-DIME}$ obtains the lowest variance, when excluding I_{CPC} from the estimators comparison (I_{CPC} should not be desirable as it is upper bounded). The illustrated results are obtained with the *joint* architecture (except for NJEE) because, when the

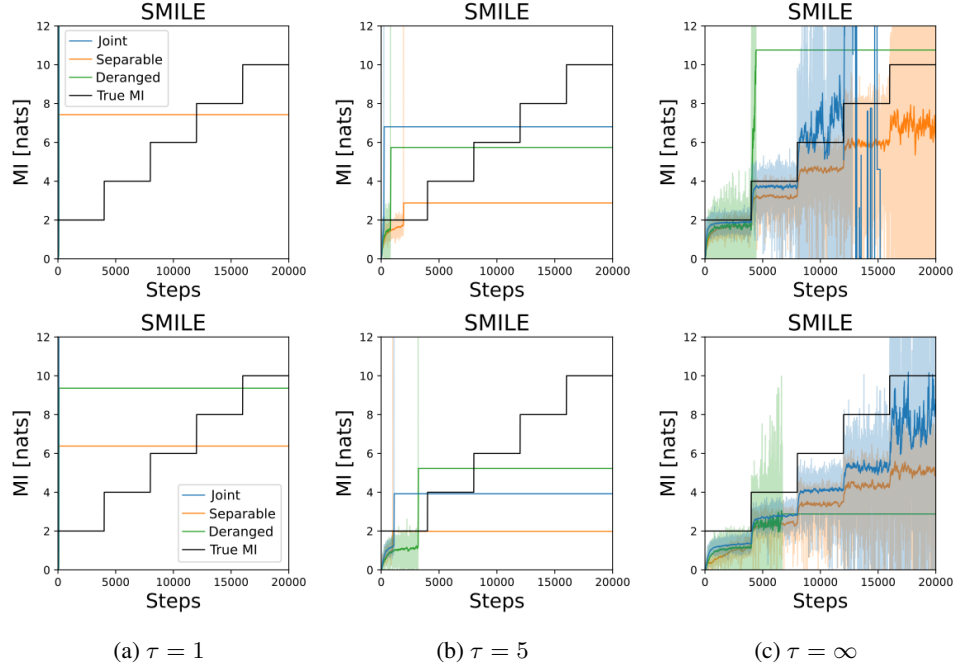


Figure 6: I_{SMILE} behavior for different values of τ , when the JS divergence is not used to train the neural network. The *Gaussian* case is reported in the top row, while the *cubic* case is reported in the bottom row.

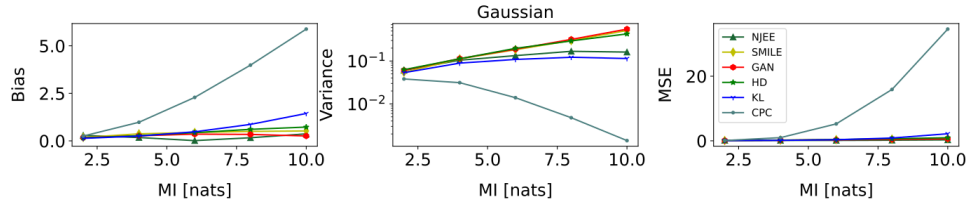


Figure 7: Bias, variance, and MSE comparison between estimators, using the joint architecture for the *Gaussian* case with $d = 20$ and $N = 64$.

batch size is small, such an architecture achieves slightly better results than the *deranged* one, as it approximates the expectation over the product of marginals with more samples.

The variance of the f -DIME estimators achieved in the *Gaussian* setting when N ranges from 64 to 1024 is reported in Fig. 10. The behavior shown in such a figure demonstrates what is stated in Lemma 3, i.e., the variance of the f -DIME estimators varies as $\frac{1}{N}$.

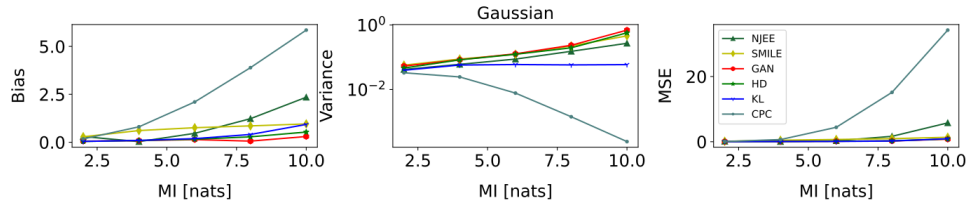


Figure 8: Bias, variance, and MSE comparison between estimators, using the joint architecture for the *Gaussian* case with $d = 5$ and $N = 64$.

Table 1: Bias, variance, and MSE of the MI estimators using the joint architecture, when $d = 20$ and $N = [512, 1024]$, for the Gaussian setting.

		Gaussian				
MI		2	4	6	8	10
Bias	NJEE	[0.42, 0.44]	[0.40, 0.42]	[0.37, 0.41]	[0.34, 0.40]	[0.32, 0.38]
	SMILE	[0.25, 0.27]	[0.48, 0.51]	[0.64, 0.67]	[0.74, 0.73]	[0.86, 0.83]
	GAN-DIME	[0.11, 0.09]	[0.15, 0.13]	[0.16, 0.12]	[0.14, 0.04]	[0.01, 0.16]
	HD-DIME	[0.08, 0.07]	[0.15, 0.12]	[0.24, 0.20]	[0.37, 0.30]	[0.47, 0.43]
	KL-DIME	[0.07, 0.06]	[0.12, 0.10]	[0.21, 0.17]	[0.38, 0.31]	[0.69, 0.56]
	CPC	[0.08, 0.05]	[0.34, 0.23]	[1.07, 0.80]	[2.32, 1.87]	[3.96, 3.37]
Var	NJEE	[0.01, 0.00]	[0.01, 0.01]	[0.02, 0.01]	[0.02, 0.01]	[0.02, 0.01]
	SMILE	[0.01, 0.01]	[0.03, 0.02]	[0.06, 0.03]	[0.11, 0.07]	[0.17, 0.11]
	GAN-DIME	[0.01, 0.01]	[0.03, 0.02]	[0.06, 0.04]	[0.11, 0.07]	[0.17, 0.12]
	HD-DIME	[0.01, 0.01]	[0.03, 0.02]	[0.05, 0.04]	[0.07, 0.06]	[0.09, 0.08]
	KL-DIME	[0.01, 0.01]	[0.01, 0.01]	[0.02, 0.01]	[0.02, 0.01]	[0.02, 0.01]
	CPC	[0.01, 0.00]	[0.01, 0.00]	[0.01, 0.00]	[0.00, 0.00]	[0.00, 0.00]
MSE	NJEE	[0.18, 0.20]	[0.18, 0.18]	[0.16, 0.18]	[0.14, 0.17]	[0.12, 0.16]
	SMILE	[0.08, 0.08]	[0.26, 0.28]	[0.47, 0.48]	[0.66, 0.61]	[0.90, 0.80]
	GAN-DIME	[0.03, 0.02]	[0.05, 0.04]	[0.09, 0.05]	[0.13, 0.08]	[0.18, 0.15]
	HD-DIME	[0.02, 0.01]	[0.05, 0.04]	[0.11, 0.08]	[0.21, 0.15]	[0.31, 0.26]
	KL-DIME	[0.01, 0.01]	[0.03, 0.02]	[0.06, 0.04]	[0.17, 0.11]	[0.49, 0.33]
	CPC	[0.01, 0.01]	[0.13, 0.06]	[1.16, 0.64]	[5.38, 3.48]	[15.67, 11.38]

Table 2: Bias, variance, and MSE of the MI estimators using the joint architecture, when $d = [5, 10]$ and $N = [64]$, for the Gaussian setting.

		Gaussian				
MI		2	4	6	8	10
Bias	NJEE	[0.30, 0.29]	[0.03, 0.13]	[0.46, 0.06]	[1.23, 0.38]	[2.35, 0.80]
	SMILE	[0.29, 0.24]	[0.61, 0.52]	[0.76, 0.68]	[0.85, 0.71]	[0.96, 0.68]
	GAN-DIME	[0.06, 0.12]	[0.09, 0.17]	[0.14, 0.17]	[0.06, 0.20]	[0.30, 0.18]
	HD-DIME	[0.04, 0.09]	[0.09, 0.14]	[0.15, 0.22]	[0.28, 0.39]	[0.53, 0.40]
	KL-DIME	[0.04, 0.07]	[0.09, 0.13]	[0.19, 0.30]	[0.40, 0.58]	[0.93, 1.05]
	CPC	[0.17, 0.20]	[0.80, 0.89]	[2.10, 2.20]	[3.89, 3.93]	[5.85, 5.86]
Var	NJEE	[0.04, 0.05]	[0.06, 0.08]	[0.09, 0.10]	[0.15, 0.13]	[0.27, 0.13]
	SMILE	[0.06, 0.06]	[0.09, 0.13]	[0.12, 0.20]	[0.23, 0.32]	[0.46, 0.46]
	GAN-DIME	[0.05, 0.06]	[0.08, 0.12]	[0.13, 0.19]	[0.24, 0.30]	[0.69, 0.52]
	HD-DIME	[0.05, 0.06]	[0.08, 0.11]	[0.12, 0.16]	[0.20, 0.24]	[0.57, 0.49]
	KL-DIME	[0.04, 0.05]	[0.06, 0.08]	[0.06, 0.10]	[0.06, 0.10]	[0.06, 0.10]
	CPC	[0.03, 0.04]	[0.02, 0.03]	[0.01, 0.01]	[0.00, 0.00]	[0.00, 0.00]
MSE	NJEE	[0.13, 0.13]	[0.06, 0.09]	[0.30, 0.10]	[1.66, 0.28]	[5.78, 0.76]
	SMILE	[0.14, 0.11]	[0.46, 0.40]	[0.70, 0.66]	[0.95, 0.83]	[1.37, 0.93]
	GAN-DIME	[0.06, 0.08]	[0.09, 0.15]	[0.15, 0.22]	[0.24, 0.34]	[0.78, 0.55]
	HD-DIME	[0.05, 0.07]	[0.09, 0.13]	[0.15, 0.21]	[0.28, 0.40]	[0.86, 0.65]
	KL-DIME	[0.04, 0.06]	[0.07, 0.10]	[0.10, 0.19]	[0.22, 0.44]	[0.92, 1.20]
	CPC	[0.06, 0.08]	[0.67, 0.83]	[4.42, 4.84]	[15.14, 15.45]	[34.22, 34.32]

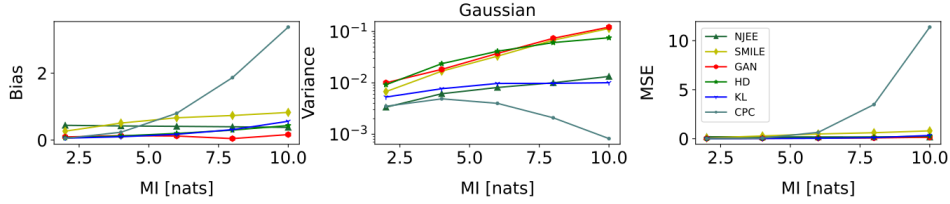


Figure 9: Bias, variance, and MSE comparison between estimators, using the joint architecture for the *Gaussian* case with $d = 20$ and $N = 1024$.

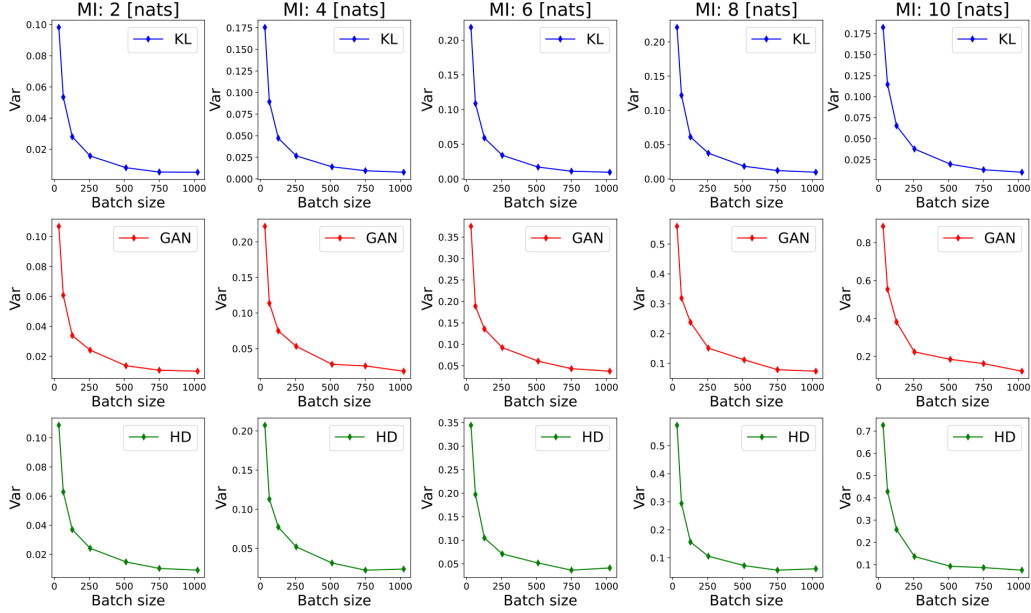


Figure 10: Variance of the f -DIME estimators corresponding to different values of batch size.

The class f -DIME is able to estimate the MI for high-dimensional distributions, as shown in Fig. 11, where $d = 100$. In that figure, the estimates behavior is obtained by using the simple architectures described in Sec. C.1 of the Appendix. Thus, the input size of these neural networks (200) is comparable with the number of neurons in the hidden layers (256). Therefore, the estimates could be improved by increasing the number of hidden layers and neurons per layer. The graphs in Fig. 11 illustrate the advantage of the architecture *deranged* over the *separable* one.

C.1.3 Derangement vs Permutation

We report in Fig. 12 an example of the difference between the derangement and permutation strategies to obtain N samples of $p_X(\mathbf{x})p_Y(\mathbf{y})$ from $p_{XY}(\mathbf{x}, \mathbf{y})$. The estimate attained by using the permutation mechanism, showed in Fig. 12b, demonstrates Theorem 2 and Corollary 2.1, as the upper bound corresponding to $\log(N)$ (with $N = 128$) is clearly visible.

C.1.4 Time Complexity Analysis

The computational time analysis is developed on a server with CPU "AMD Ryzen Threadripper 3960X 24-Core Processor" and GPU "MSI GeForce RTX 3090 Gaming X Trio 24G, 24GB GDDR6X". Before analyzing the time requirements to complete the 5-step MI staircases, we specify two different ways to implement the derangement of the y realizations in each batch:

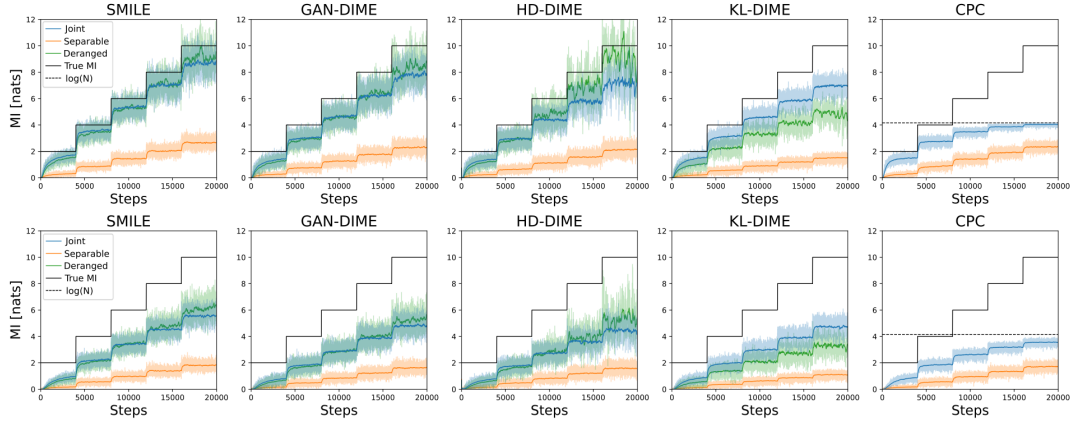
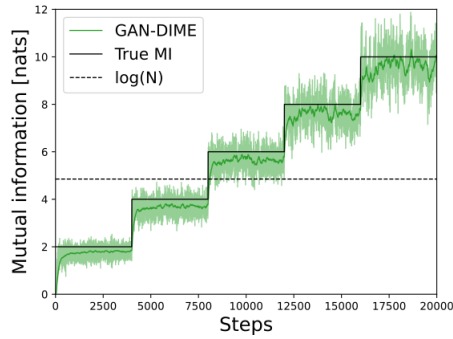
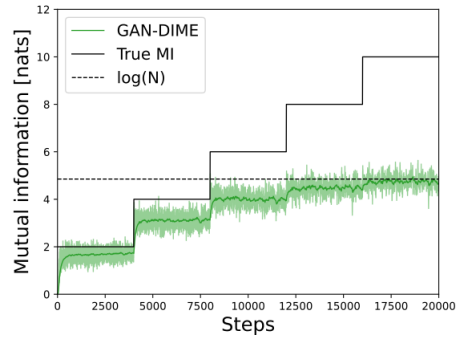


Figure 11: MI estimates when $d = 100$ and $N = 64$. The *Gaussian* setting is represented in the top row, while the *cubic* setting is shown in the bottom row.



(a) Derangement training strategy example.



(b) Random permutation training strategy example.

Figure 12: Comparison between derangement and permutation training procedures, for $d = 20$ and $N = 128$.

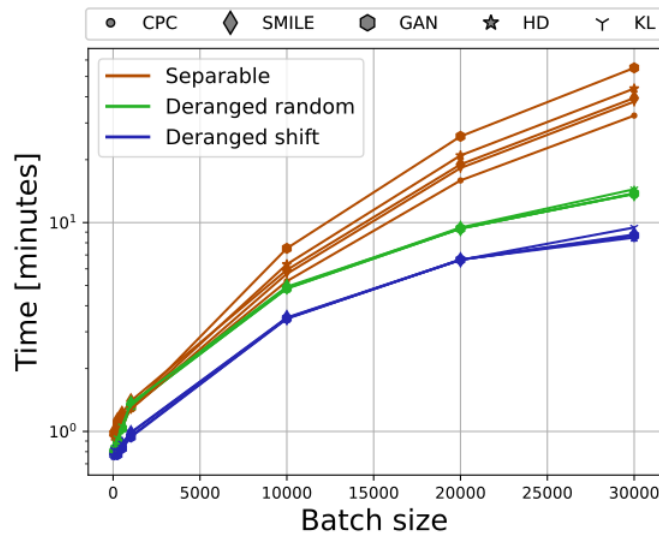


Figure 13: Comparison between the time requirements to complete the 5-step staircases for the architectures *separable*, *deranged* with random-based derangement, and *deranged* with shift-based derangement.

Table 3: Summary of the MI estimators.

Estimator	Low MI		High MI		Scalability
	Bias	Variance	Bias	Variance	
$I_{KL-DIME}$	✓✓	✓✓	~	✓✓	✓✓
$I_{HD-DIME}$	✓✓	✓✓	✓	✓	✓✓
$I_{GAN-DIME}$	✓✓	✓✓	✓✓	✓	✓✓
$I_{SMILE}(\tau = 1)$	✓	✓✓	✓	✓	✓✓
I_{NJEE}	✓	✓✓	✓	✓✓	✗
I_{CPC}	~	✓✓	✗	✓✓	✗
$I_{SMILE}(\tau = \infty)$	✓	~	✓	✗	✓✓
I_{MINE}	✓	✗	✗	✗	✓✓
I_{NWJ}	✓	✗	✗	✗	✓✓

- **Random-based.** The trivial way to achieve the derangement is to randomly shuffle the elements of the batch until there are no fixed points (i.e., all the \mathbf{y} realizations in the batch are assigned to a different position w.r.t. the starting location).
- **Shift-based.** Given N realizations $(\mathbf{x}_i, \mathbf{y}_i)$ drawn from $p_{XY}(\mathbf{x}, \mathbf{y})$, for $i \in \{1, \dots, N\}$, we obtain the deranged samples as $(\mathbf{x}_i, \mathbf{y}_{(i+1)\%N})$, where "%" is the modulo operator.

Although the MI estimates obtained by the two derangement methods are almost indistinguishable, all the results shown in the paper are achieved by using the random-based method. We additionally demonstrate the time efficiency of the shift-based approach.

We show in Fig. 4 that the architectures *deranged* and *separable* are significantly faster w.r.t. *joint* and *NJEE* ones, for a given batch size N and input distribution size d .

However, Fig. 4 exhibits no difference between the *deranged* and *separable* architectures. Fig. 13 illustrates a detailed representation of the time requirements of these two architectures to complete the 5-step stairs presented in Sec. 6. As N increases, the gap between the time needed by the architectures *deranged* and *separable* grows, demonstrating that the former is the fastest. For example, when $d = 20$ and $N = 30k$, $I_{GAN-DIME}$ needs about 55 minutes when using the architecture *separable*, but only 15 minutes when using the *deranged* one and less than 9 minutes for the shift-based *deranged* architecture.

C.1.5 Summary of the Estimators

We give an insight on how to choose the best estimator in Tab. 3, depending on the desired specifics. We assign qualitative grades to each estimator over different performance indicators. All the indicators names are self-explanatory, except from *scalability*, which describes the capability of the estimator to obtain precise estimates when d and N vary from the default values ($d = 20$ and $N = 64$). The grades ranking is, from highest to lowest: ✓✓, ✓, ~, ✗. When more than one architecture is available for a specific estimator, the grade is assigned by considering the best architecture within that particular case.

Even though the estimator choice could depend on the specific problem, we consider $I_{GAN-DIME}$ to be the best one. The rationale behind this decision is that $I_{GAN-DIME}$ achieves the best performance for almost all the indicators and lacks weaknesses. Differently, I_{CPC} estimate is upper bounded, I_{SMILE} achieves slightly higher bias, and I_{NJEE} is strongly d and N dependent. However, if the considered problem requires the estimation of a low-valued MI, $I_{KL-DIME}$ is slightly more accurate than $I_{GAN-DIME}$.

One limitation of this paper is that the set of f -divergences analyzed is restricted to three elements. Thus, probably there exists a more effective f -divergence which is not analyzed in this paper. In addition, not all f -divergences can be used for representation learning and capacity approaching algorithms, as the double maximization of each cost function does not necessarily correspond to the maximization of the MI.

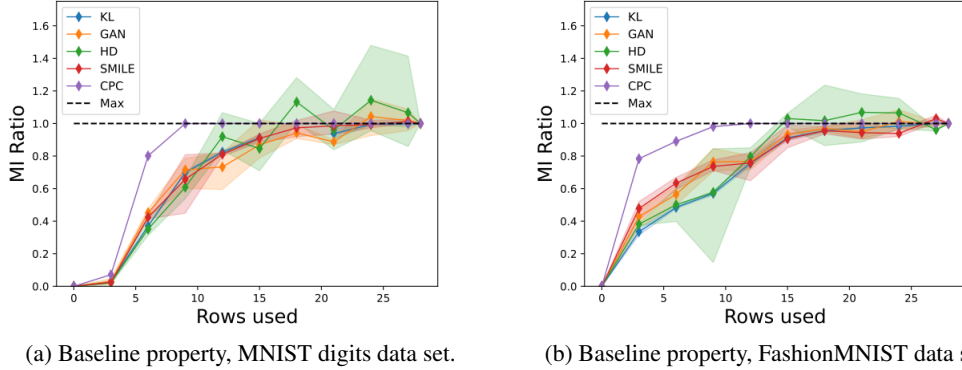


Figure 14: Comparison between different estimators for the baseline property, using MNIST data set on the left and FashionMNIST on the right.

C.2 Self-Consistency Tests

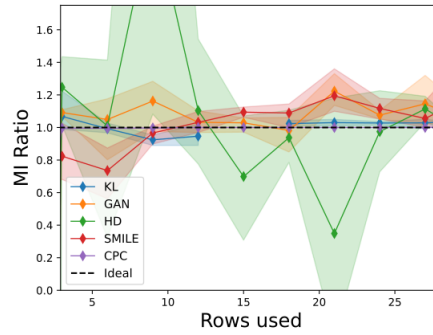
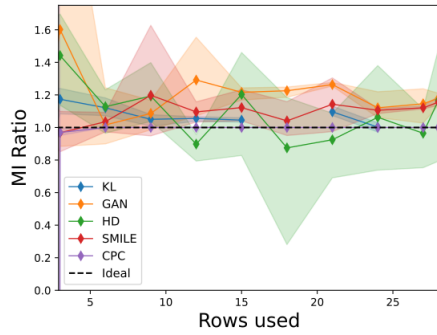
The benchmark considered for the self-consistency tests is similar to the one applied in prior work [18]. We use the images collected in MNIST [28] and FashionMNIST [29] data sets. Here, we test three properties of MI estimators over images distributions, where the MI is not known, but the estimators consistency can be tested:

1. **Baseline.** X is an image, Y is the same image masked in such a way to show only the top t rows. The value of $\hat{I}(X; Y)$ should be non-decreasing in t , and for $t = 0$ the estimate should be equal to 0, since X and Y would be independent. Thus, the ratio $\hat{I}(X; Y)/\hat{I}(X; X)$ should be monotonically increasing, starting from 0 and converging to 1.
2. **Data-processing.** \bar{X} is a pair of identical images, \bar{Y} is a pair containing the same images masked with two different values of t . We set $h(Y)$ to be an additional masking of Y of 3 rows. The estimated MI should satisfy $\hat{I}([X, X]; [Y, h(Y)])/ \hat{I}(X; Y) \approx 1$, since including further processing should not add information.
3. **Additivity.** \bar{X} is a pair of two independent images, \bar{Y} is a pair containing the masked versions (with equal t values) of those images. The estimated MI should satisfy $\hat{I}([X_1, X_2]; [Y_1, Y_2])/ \hat{I}(X; Y) \approx 2$, since the realizations of the X and Y random variables are drawn independently.

These tests are developed for I_{fDIME} , I_{CPC} , and I_{SMILE} . Differently, I_{NJEE} training is not feasible, since by construction $2d - 1$ models should be created, with $d = 784$ (the gray-scale image shape is 28×28 pixels). The neural network architecture used for these tests is referred to as **conv**.

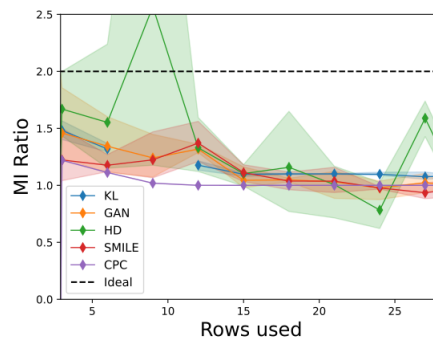
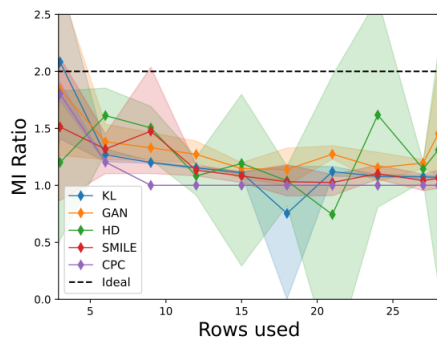
Conv. It is composed by two convolutional layers and one fully connected. The first convolutional layer has 64 output channels and convolves the input images with (5×5) kernels, stride $2 px$ and padding $2 px$. The second convolutional layer has 128 output channels, kernels of shape (5×5) , stride $2 px$ and padding $2 px$. The fully connected layer contains 1024 neurons. ReLU activation functions are used in each layer (except from the last one). The input data are concatenated along the channel dimension. We set the batch size equal to 256.

The comparison between the MI estimators for varying values of t is reported in Fig. 14, 15, and 16. The behavior of all the estimators is evaluated for various random seeds. These results highlight that almost all the analyzed estimators satisfy the first two tests ($I_{HD-DIME}$ is slightly unstable), while none of them is capable of fulfilling the additivity criterion. Nevertheless, this does not exclude the existence of an f -divergence capable to satisfy all the tests.



(a) Data processing property, MNIST digits data set. (b) Data processing property, FashionMNIST data set.

Figure 15: Comparison between different estimators for the data processing property, using MNIST data set on the left and FashionMNIST on the right.



(a) Additivity property, MNIST digits data set.

(b) Additivity property, FashionMNIST data set.

Figure 16: Comparison between different estimators for the additivity property, using MNIST data set on the left and FashionMNIST on the right.